Influence of the cathode material in the cathode fall characteristics of a hydrogen hollow cathode glow-discharge

V. Gonzalez-Fernandez, K. Grützmacher, C. Pérez, M. I. de la Rosa
Dpto. de Física Teórica, Atómica y Óptica, Universidad de Valladolid, Paseo Belén 7, 47011, Valladolid, Spain
E-mail: veronica.gonzalez.fernandez@uva.es

Abstract. In this work, we present Doppler free two photon optogalvanic measurement to determine the local electric field strength (E-field) in the cathode fall region of a hollow cathode discharge, operated in pure hydrogen, via the Stark splitting of the 2S level of hydrogen. The main aim of this article is the comparison of the measurements made with different cathode materials, stainless steel and tungsten, both of them widely used in low-pressures discharges. Sputtering of stainless steel is the principle cause of the differences observed for the E-field variation, and the differences are analysed in the frame of the sputtered material in a wide range of discharge conditions. Complementary images of the discharge luminosity allow for the conclusion; that the cathode dark zone corresponds in good approximation to the cathode fall length.

1. Introduction

Low temperature plasmas, usually far of thermodynamic equilibrium, have been studied since many decades and this trend still continues, see e.g. [1-5], because many of those plasmas are of technological relevance or related to industrial applications. However, a deep understanding of the corresponding plasma characteristics is still missing. According to the large sort of plasma conditions generated in dc, pulsed or RF discharges and different geometrical configurations, many experimental techniques are employed to study important plasma parameters: kinetics gas temperature, neutral and charged particle density, lines shapes, energy distributions, etc [6,7]. A relevant discharge characteristic is the local electric field strength (E-field), because it dominates charged particle fluxes, their energy distributions functions and the charge densities. Over the years, various strategies have been developed to measure the E-field present in different kind of discharges: RF discharges, plasma jets, etc... Laser spectroscopic techniques can provide high spatial and temporal resolution employing nanosecond light pulses and moderate irradiances. Most E-field measurements are based in Stark splitting, shifting and mixing of the Rydberg states of different atomic and molecular species, using any kind of emission spectroscopy or active laser spectroscopy, see for instance [8-22].

In general, it is fairly difficult to compare the results obtained for different experimental conditions related to discharge design and geometry, as well as discharge conditions given by carrier gas, current and pressure, cathode material, etc. For these reasons, the possibility of comparing experimental results obtained for the same discharge conditions, while varying the cathode material and diameter, offers the opportunity to study the impact of these changes on the cathode fall characteristics. This article is focused in the comparison of the E-field measurements made with two cathode materials, stainless steel and tungsten, both of them widely used in low-pressures discharges. As will be seen in this paper, the cathode material will have an important influence on the plasma characteristics due to sputtered material; see ref. [23-28].

Beside of various buffer or carrier gases that can be used, hydrogen is of particular interest, because it plays an important role in several plasmas technological processes due to its pronounced chemical reactivity. For many years our group has studied E-field strength in a hollow cathode hydrogen discharge using two Doppler-free laser spectroscopy techniques: two-photon polarization spectroscopy [29] and optogalvanic spectroscopy [30-33] based on the Stark splitting of the 1S-2S hydrogen transition. In general, in optogalvanic spectroscopy the detection system does not require a complex experimental arrangement. Nevertheless, it can provide exceptional high spatial resolution: e.g. 80 %

of the signal is generated in a tiny excitation volume of 100 µm in diameter and 10 mm length [34].

Our experimental arrangement includes a versatile hollow cathode discharge (HCD), where the cathode diameter and material can be easily changed. In a first measurement campaign two tungsten cathodes of 10 and 15 mm of inner diameter [32] allowed us to study the influence of the cathode diameter on the cathode fall characteristics. It turned out that the cathode fall does not depend on the geometry operating the discharge with equal current density for both cathode diameters keeping all other discharge parameters fixed. Therefore the measurements of our tungsten HCD serve as cathode fall reference to be compared with plane-parallel electrodes discharges [35-39], and they are also valid to test one-dimensional models.

The second measurement campaign using stainless steel cathodes - presented in this paper - is dedicated to study if the cathode material may have an influence on the cathode fall characteristics by comparing the cathode fall of the tungsten HCD with those obtained for stainless steel. However, a previous study revealed, that E-field determination in stainless steel is extremely sensitive with respect to the irradiance of the laser radiation (which corresponds to the laser pulse energy) in the excitation volume, because increasing irradiance causes erroneously higher E-field strengths for stainless steel cathode not observed for tungsten [33]. This phenomenon is almost certainly related to sputtering rate of stainless steel, which is estimated to be 10^4 times larger than in tungsten [40], because the plasma in the vicinity of the cathode may be remarkably contaminated. This previous study was very important for reliable E-fields determination for the stainless steel, which requires a much more restricted irradiance limitation; hence the laser pulse energy control is indeed crucial.

This article describes shortly in Section 2 the experimental arrangement and the measurement procedure, the recorded Stark spectra and the determination of the corresponding local E-field values. In Section 3 the cathode fall characteristics determined for two stainless steel cathodes of different inner diameters (10 and 15 mm) are compared in order to study the influence of the cathode geometry. The most extended part of the article is Section 4; comparing the entire cathode fall characteristics obtained for tungsten and stainless steel cathodes in a wide range of discharge conditions. Related data, like the maximum E-field present at the cathode surface and the length of the cathode fall extension (cathode dark space) are presented. Finally, the perturbation of the cathode fall characteristics due to sputtering is studied.

2. Experimental arrangement, measurements and E-field determination

The whole experimental arrangement is widely explained elsewhere [32], so here we only give the most important details. The plasma source is a home-made hollow cathode discharge (HCD), operated with pure hydrogen in *abnormal glow* regime. The central hollow cathode has a length of 50 mm and is placed between two cone-peaked stainless steel anodes. This design provides a symmetrical discharge with excellent long and short term stability of the discharge impedance, which is crucial for the background signal in optogalvanic detection. Different cathodes made of tungsten or stainless steel and with two different inner diameters (10 or 15 mm) can be inserted. Anodes and cathode are placed in a water-cooled outer brass structure. All pieces are electrically isolated and the anodes have off axis axial perforation for end-on spectroscopic measurements. A continuous gas flow of about 10 cm^3s^{-1} is entering at one anode and leaving at the opposite one. The discharge is operated in a wide range of pressures and currents, from 400 to 1350 Pa, and from 50 to 300 mA, leading to E-field strengths up to 4.5 kV/cm close to the cathode surface.

The entire discharge voltage (V_d) vs discharge current, i:e. the voltage-current characteristic curves, are

quite similar for stainless steel and tungsten cathodes[32] for the same current and pressure range. The positive slope indicates that the discharge is operated in *abnormal glow* regime. V_d is only slightly higher for the stainless steel cathodes when cathode sputtering becomes considerable, i.e. higher discharge current and lower pressure. Further analysis will be shown in Section 4.

Reliable laser spectroscopic measurements presented in this paper require tuneable UV-laser radiation with exceptional characteristics. Up to now commercial laser systems cannot provide such radiation. Therefore in our laboratory, we started already more than two decades ago to develop advanced pulsed single longitudinal mode (SLM), UV-laser spectrometers, especially suited for laser-aided plasma diagnostic. The present system consists of a 10 Hz injection-seeded Q-switched Nd:YAG laser (Continuum, Powerlite 9000) and a modified OPO-KTP, OPA-BBO system (Continuum, Mirage 500) including additional sum-frequency generation (SFG-BBO) crystal. The whole chain of non-linear processes involved had to be optimized for high conversion efficiency, stability and reliable operation. This concept provides tuneable laser radiation around 243 nm, up to 10 mJ pulse energy, single longitudinal mode operation, 2.5 ns pulse duration and a 300 MHz bandwidth. The beam divergence is less than 100 µrad. The pulse energy conversion efficiency from the infrared output of the Nd:YAG laser into tuneable UV-radiation is about 2%. Since the OPO reduces the pulse duration by a factor of three, the pulse peak power conversion efficiency is as higher as 5%.

To verify the spectral quality and the regular tuning of the laser emission while recording the spectra, the OPO signal is controlled by a monitor etalon with free spectral range (FSR) about 7 GHz and a photodiode. The standard deviation of the fringe separation for the most usual sets of measurements is about 160 MHz, half of the laser bandwidth.

High resolution Doppler-free two-photon absorption measurements were performed by optogalvanic detection. Following the selection rules of the two-photon excitation for the 1S-2S hydrogen transition ($\Delta L = 0$), two opposite circularly polarized laser beams were focused with 1 m focal length lenses in the measurement volume. The counter-propagating laser beams are crossing in the horizontal plane; and the beams overlap is aligned parallel to the cathode surface, and centred with respect to the cathode length [33]. To achieve this, the discharge source is mounted in two linear translators. The horizontal one provides a good alignment control for the counter-propagating laser beams. The vertical allows performing the measurements at different distances from the cathode surface. The closest measurements were taken at 160 µm from the cathode surface limited by the device geometry. The overlap volume is controlled in real time by spatial profile analyser LaserCam-HR-UV.

The signal recorded via optogalvanic spectroscopy is caused by the simultaneous absorption of the two photons, followed by photo-ionization due to the absorption of a third photon. This induces a tiny change in the impedance of the discharge that can be detected as a transient voltage drop between the cathode and one anode. Recent calculations based on first principles [34] allowed us to determine the three-dimensional photo-ionization yield in the excitation volume. The study revealed an extraordinary high spatial resolution, because 80 % of the optogalvanic signal comes from the overlap volume of only 100 µm in diameter and 10 mm length, at moderate laser pulse energy of 45 µJ, i.e. irradiance of 150 MW/cm^2. Varying the pulse energy, the signal can suffers saturation due to depletion of the atomic ground state density and the life time reduction of the 2S level due to photo-ionization. A previous study [33], demonstrated that for tungsten cathode the signal saturation produces only an additional broadening of the Stark components which does not affect therefore the E-field determination. On the other hand, exceeding a certain maximum irradiance using stainless steel cathodes causes additionally a pronounced shifting of the Stark components, which results in erroneous higher E-field strengths. This is referred to the sputtering rate, which is about 10^4 times larger for stainless steel compared to

tungsten [40]. Therefore, reliable E-field determination in stainless steel cathodes requires a very rigorous control of the laser pulse energy and of the laser beam focus.

In figure 1 several typical spectra recorded close to the cathode surface are shown for a 10 mm stainless steel cathode, operated at a pressure of 400 Pa and a current of 50 mA. The E-field present in the cathode region causes the Stark splitting and shifting of the 2S level of hydrogen [29]. The recorded spectra have three characteristics peaks, corresponding to the $2P^{1/2}$, $2S^{1/2}$ and the $2P^{3/2}$ components. The exceptional narrow bandwidth of the laser (300 MHz) allows resolving the hyperfine structure of each Stark component, as can be seen in figure 1. The frequency separation measured between the $2P^{1/2}$ (red) and the $2P^{3/2}$ (blue) components i.e. ($\Delta\nu=\nu(2P^{1/2})-\nu(2P^{3/2})$) is compared with the theoretical predictions [29] to determine the local E-field value. Obviously, with increasing distance from the cathode surface the E-field decreases and the components become closer. The intensity of the signal decreases with the distance from the cathode surface due to the optogalvanic detection. In figure 1 the choice of the 0 GHz value is not relevant; it was fixed in the hyperfine component of the central ($2S^{1/2}$) one.

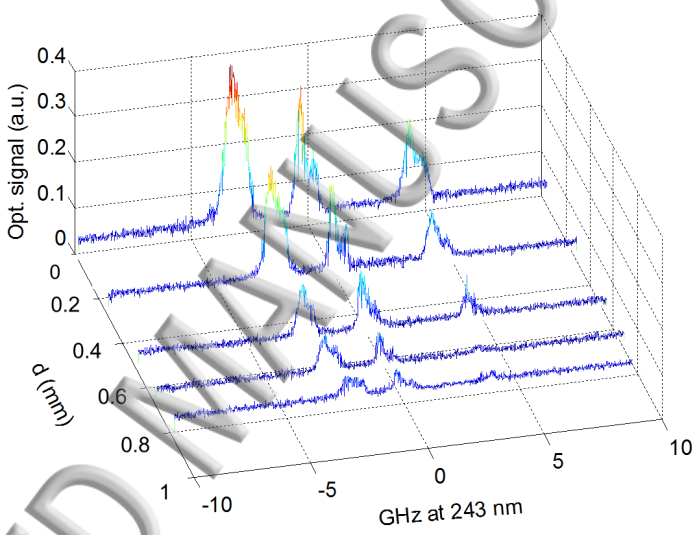

Figure 1: Set of raw data taken at different distances from the cathode surface (d) in a 10 mm stainless steel cathode, at a pressure of 400 Pa and 50 mA current.

3. E-field variation with current density in stainless steel cathodes of different diameters

The previous measurement campaign using tungsten cathodes [32] revealed that the cathode fall characteristics, i.e. the variation of the E-field strength with distance from the cathode surface, do not depend on the cathode diameter. This means that our measurements, performed in a particular discharge design, can be directly compared with other discharge geometries. Before starting with the comparison between the two different cathode materials, it is reasonable to check first if the same conclusion is also valid for stainless steel cathodes; using the same current densities than in tungsten cathodes (3.18, 6.37 and 9.55 mA/cm^2), with two different inner diameters (10 and 15 mm). However, for stainless steel cathodes, reliable optogalvanic measurements were not possible for the same wide range of the discharge conditions as for tungsten, because the short term stability of the discharge impedance, i.e. signal noise is worse. This is referred to the much larger sputtering rate for stainless steel, which can cause inhomogeneous contamination of the hydrogen plasma resulting in short time

discharge instabilities. This increases dramatically the noise of the background signal and prevents high spatial resolution optogalvanic detection.

Figure 2 shows all the possible comparisons for stainless steel cathodes for the two diameters. For better clearness, each plot shows the E-field strength vs distance from the cathode surface for a fixed pressure and current density, indicated in the figure. Parabolic or linear fits have been applied to the experimental data. For both diameters the behaviour is quite similar, following the same conclusion than in the previous work with tungsten cathode [32], i.e., the cathode diameter has only little influence on the cathode fall characteristics. However, due to sputter material, this does not conclude, that stainless steel cathode can provide pure hydrogen plasma as found for tungsten cathodes. Therefore, a more detailed analysis will be presented in section 4.

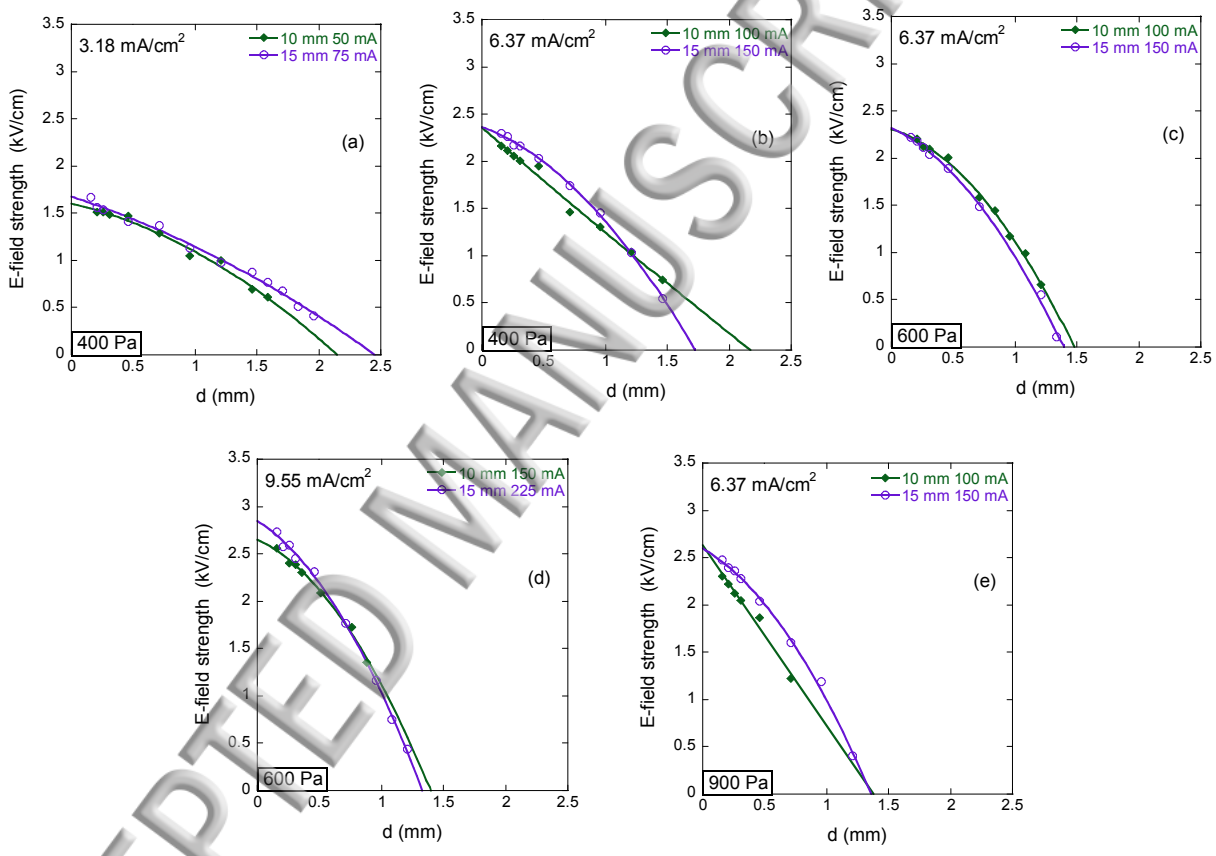

Figure 2: E-field strength vs radial distance from the cathode surface in two stainless steel cathodes, for cathode diameters of 10 and 15 mm and different current densities (3.18, 6.37 and 9.55 mA/cm^2).

4. Comparison of cathode fall characteristics for stainless steel and tungsten cathodes

To study the influence of the cathode material E-field measurements performed in stainless steel cathodes, are compared with recent results obtained for tungsten cathodes [32]. For the comparison only the measurements in 15 mm cathodes are shown (section 4.1), just because reliable optogalvanic measurements were possible in a wider range of discharge parameters. Nevertheless, the behaviour in 10 mm cathodes is very similar. In section 4.2, the variation of the maximum E-field and the length of the cathode fall (d_{cf}) are analysed with pressure and current. In section 4.3 the cathode fall characteristics are linked to cathode sputtering. To complete the analysis images of the discharge

luminosity are shown in section 4.4, which allow some interesting conclusion.

4.1 E-field strength variation.

In figure 3 stainless steel and tungsten E-field strengths measured in 15 mm cathodes are plotted together for comparison. In the figure, each row corresponds to the same pressure, and each column to the same discharge current. Each E-field value is plotted with its error bar, resulting from the small lack of regularity of the laser frequency tuning, controlled with an etalon.

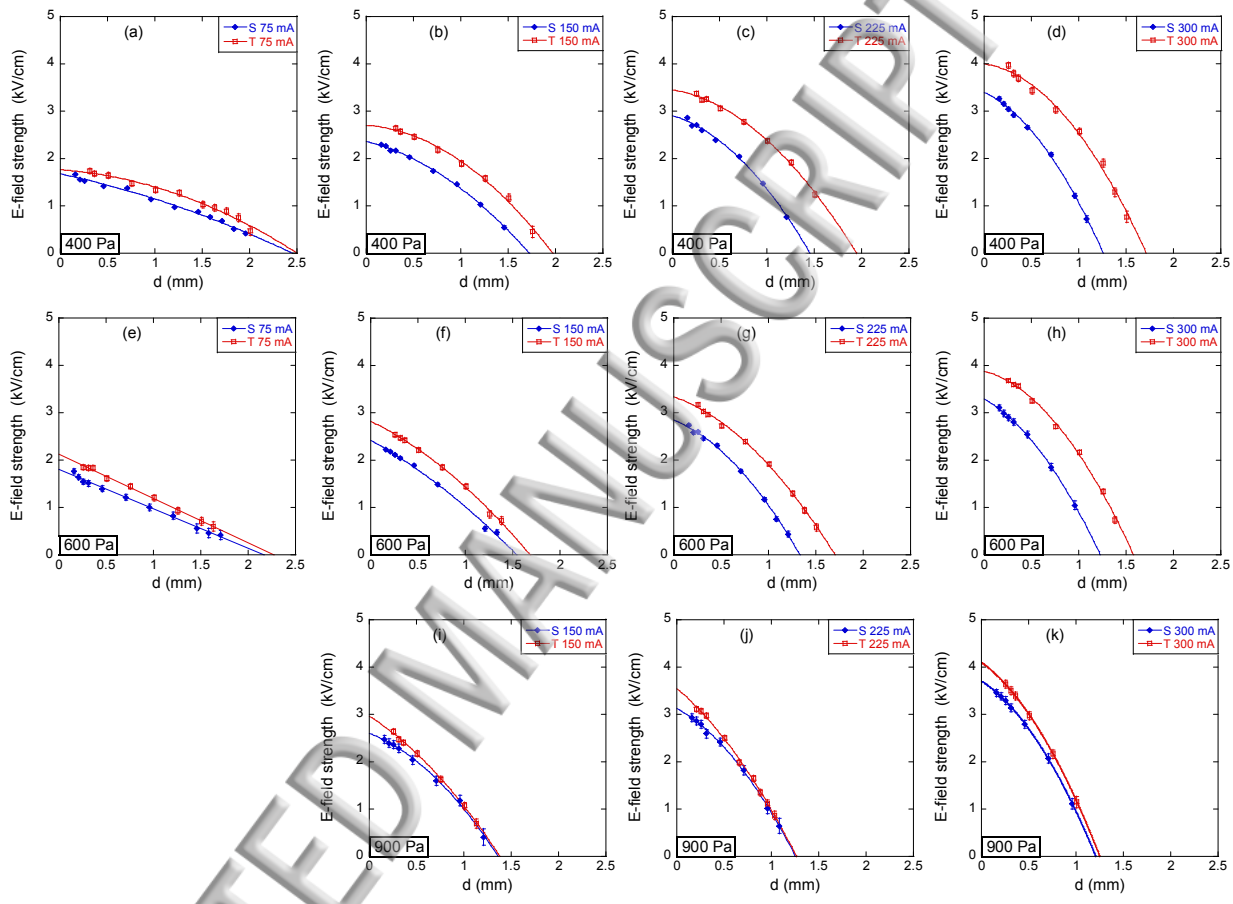

Figure 3: E-field strength vs radial distance from the cathode surface for stainless steel (S) and tungsten (T) cathodes, with 15 mm inner diameter.

This comparison shows very clearly some general tendencies. The E-field strength is always higher for tungsten than for stainless steel, and the cathode fall length d_{cf} decreases with pressure and current. For 400 and 600 Pa the curves for the two cathode materials become remarkably separated with increasing current. Nevertheless, for 900 Pa the cathode falls are very similar for both cathode materials and all discharge currents.

4.2. Analysis of maximum E-field strength and cathode fall length

The E-field measurements presented before allow obtaining the tendency of some important parameters like the maximum E-field (E_{max}) at the cathode surface, taken from the fits in figure 3, and the length of the cathode fall region (d_{cf}) with respect to discharge conditions and cathode material. All tendencies are plotted for 15 mm cathode diameter, and a similar behaviour is observed for 10 mm

diameter.

In figure 4 (a), E_{max} is shown depending on discharge current for all pressures, and the plot (b) shows E_{max} depending on pressure for all currents. For both cathode materials and all discharge pressures E_{max} increases linearly with the current, and for 400 and 600 Pa the fits are crossing, while E_{max} is always larger for 900 Pa. In figure 4 (b), attending to the variation with pressure for stainless steel and for the currents of 150, 225 and 300 mA (solid lines) the maximum presents a concave curve, with a slight minimum at 600 Pa. This trend also appears for tungsten (dotted line) at 225 and 300 mA, whereas for lower currents of 150 and 75 mA the trend is almost linear. A quite remarkable coincidence is the fact that the curve described by stainless steel, at 300 mA, is practically reproduced by tungsten, at 225 mA.

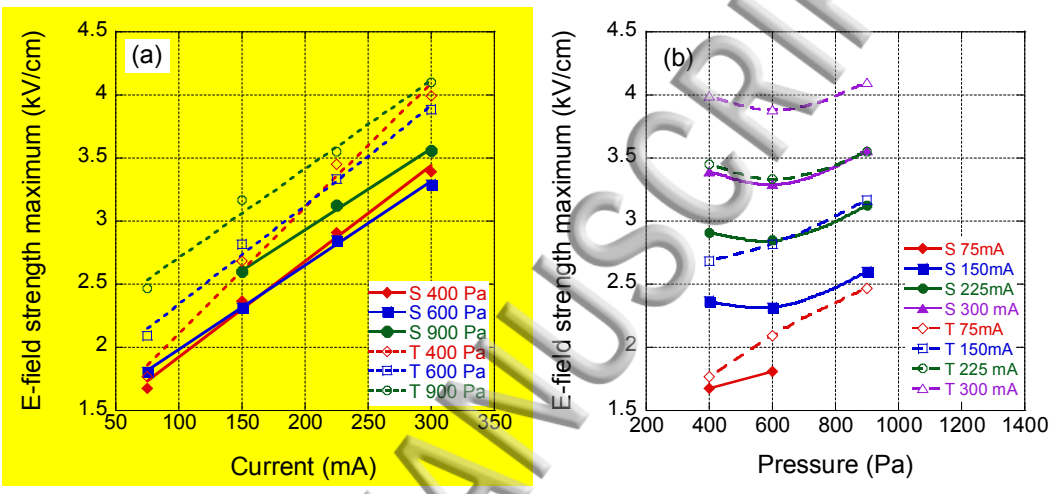

Figure 4: E_{max} (a) vs applied current and (b) vs pressure, for stainless steel (S) and tungsten (T) cathodes with an inner diameter of 15 mm.

The length of the cathode fall region (d_{cf}) is also an interesting parameter because it gives valuable information about the discharge. As can be seen in figure 3, d_{cf} decreases with increasing pressure and current, being always larger for tungsten cathodes. Corresponding tendencies are shown more detailed in figure 5 for both cathode materials. Plot (a) shows d_{cf} vs current for all pressures, and plot (b) exhibits the dependence of d_{cf} on pressure for all currents. In figure 5(a) d_{cf} decreases sharply from 75 to 150 mA for both materials at for pressures of 400 and 600 Pa. For stainless steel, the fall slows down with increasing current and pressure. For tungsten, in the range from 150 and 225 mA d_{cf} is almost constant. For the highest pressure of 900 Pa the slope is quite the same for both cathode materials. In figure 5 (b), the d_{cf} decreases linearly for all discharge conditions. In general, with increasing current the slope of the fits decreases, until the limit of stainless steel 300 mA where the d_{cf} is nearly constant with the pressure. For 75 mA the difference between both cathode materials is not very pronounced, but the separation becomes larger with current.

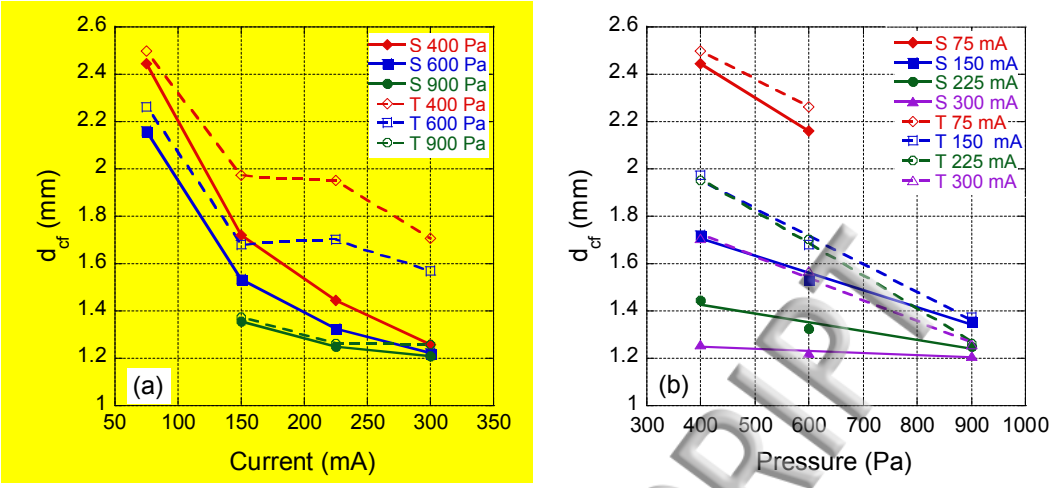

Figure 5: Length of the cathode fall region (d_{cf}) obtained from the fits in figure 3 for 15 mm cathode diameter (a) vs applied current and (b) vs pressure.

4.3 Evidence of sputtering

Before going into details, it is important to remind, that a constant flow of hydrogen is applied to the discharge to extract the sputtered material, i.e. to minimize the contamination and to maintain stable discharge conditions. Our HCD design provides a laminar hydrogen flow; hence the gas flow velocity is zero along the cathode surface and increases parabolic towards its maximum on axis. Therefore, in general the contamination of the hydrogen plasma due to sputtered material is much larger close to the cathode surface and decreases toward the central plasma.

In general, the understanding of cathode fall characteristics is quite difficult, and becomes even more complex if cathode sputtering has to be taken into account [26, 41-45]. However, some parameters allow for a simple evaluation, how the hydrogen plasma of the HCD, suffers perturbation due to sputtered iron (stainless steel) and tungsten. In a good approximation sputtering of tungsten is negligible compared to stainless steel, because it is estimated to be 10^4 times larger for stainless steel [40]. Additionally, the diffusion into the plasma is 7 times faster for iron, because of the large difference of atomic mass: being 26 for iron and 184 for tungsten. Another important parameter is the difference of the ionization potential, which is 13.6 eV (15.4 eV) for atomic (molecular) hydrogen, and about 7.9 eV for iron and tungsten. Therefore, sputtered atoms are more easily ionized than hydrogen and only those ions have an explicit influence on the cathode fall characteristics, because they increase the conductivity which reduces the voltage necessary to drive the discharge current. Without doubt, sputtering increases with discharge current, i.e. for constant discharge pressure the d_{cf} becomes reduced noticeable. This can be seen for all discharge pressures and all discharge currents in figure 3. Obviously, this tendency becomes more pronounced for the lowest discharge pressure of 400 Pa, because of various reasons. In zero order approximation, the mean free path of the ions attracted towards the cathode increases with decreasing pressure, hence the effect of the sputtering should be more evident. Furthermore, lower pressures facilitate the diffusion of the sputtered iron into the plasma. The diffusion scales with 1/n (n the density). This explains why the differences of the cathode fall characteristics nearly vanish at 900 Pa although the differences increase little with discharge current.

In figure 6 the cathode fall voltage (V_c) obtained from the integral of the E-field variation of the cathode fall are represented versus the normalized current density, in the usual units of A/Torr^{2}cm^2.

The different slopes obtained for tungsten and stainless steel cathodes confirm the conclusions above: the perturbation of the cathode fall due to sputtering increases with lower pressure and increasing current. According to this figure we concluded, that sputtering of stainless steel cathodes used for hydrogen discharges is nearly negligible for normalized current densities remarkably smaller than e.g. 10^{-4} A/Torr^{2}cm^2.

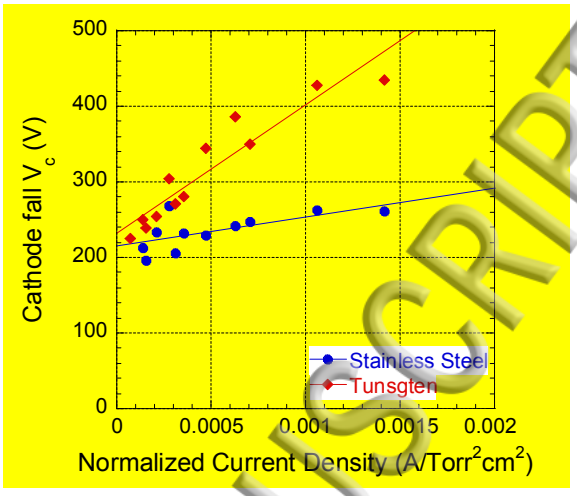

Figure 6: Cathode fall voltage (V_c) obtained from the integral of the E-field falls vs normalized current density, for stainless steel and tungsten.

4.4 Comparison of discharge luminosity with cathode fall length

To complete our study of the cathode fall characteristics, end on photographs of the discharge luminosity have been taken from one anode side for both cathode materials and diameters in the wide range of discharge conditions. For better understanding, figure 7 (a) shows one anode holder (brass) with all connections for water cooling, gas and current supplies. The cone shaped stainless steel anode has drill holes in the upper and lower part for the end-on laser-spectroscopic measurements. The red arrow indicates the laser beam in and output, and the "burned" peak of the anode indicates the stable anode current spot. Figure 7 (b) shows typical recorded discharge luminosity. The central yellow circle corresponds to a cathode diameter of 15 mm and the green circles indicate the anode with its drill holes. The shadow in the middle of the picture corresponds to the shape of the peaked anode.

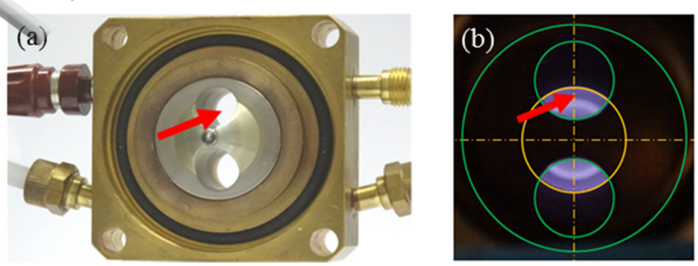

Figure 7: (a) Anode holder with inserted cone shaped stainless steel anode, viewed from the cathode side. (b) Typical discharge luminosity, with anode and its drill holes (green) and cathode (yellow). The red arrow indicates the laser beam in and output.

Figure 8 shows various pictures of the discharge luminosity, for three discharge pressures, and two discharge currents in stainless steel (S) and tungsten (T) cathodes. The images were taken with

This manuscript was accepted by J. Appl. Phys. Click here to see the version of record.

commercial camera; and the luminosity represents therefore mainly the visible spectral region. The discharge luminosity depends barely on the cathode material, but clearly on discharge conditions. The different discharge zones, usually observed in linear glow discharges, are compressed towards the circular cathode. With increasing pressure and decreasing current the circular discharge structure appears more defined, see 900 Pa and 150 mA. Although cathode fall length is not the same for both cathode materials, this behaviour cannot be detected visually, because the intensity emission is almost the same when the discharge is operated in the same conditions for both materials.

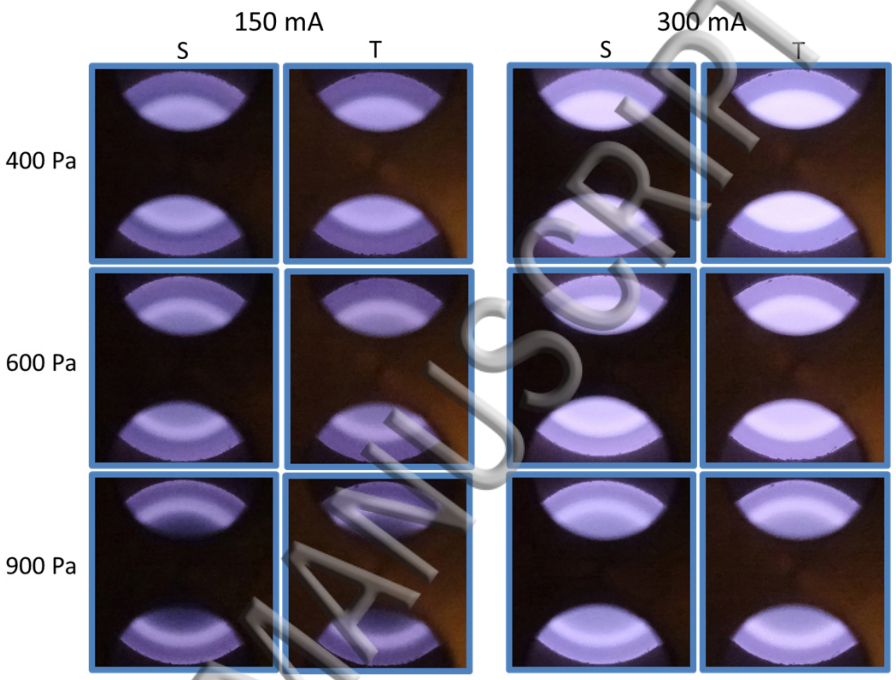

Figure 8: Luminosity taken for the discharge using stainless steel (S) and tungsten (T) cathodes, for three pressures and two currents.

A very interesting result comes from the comparison of the discharge luminosity with the precise cathode fall length obtained from figure 3. An example is shown in figure 9 for 400 Pa and two discharge currents: 150 mA (figure 9 (a)) and 300 mA (figure 9 (b)). Both images are a composition of luminosity obtained from stainless steel cathode (S, left side) and tungsten (T, right side). The red arrows correspond to the cathode fall length (d_{cf}) of tungsten obtained from figure 3, and the yellow ones to stainless steel. As mentioned above, for all measurements the luminosities observed for both materials cannot be distinguish. For tungsten cathodes the measured d_{cf} (red arrows) and the length of the dark zones observed in the luminosities agree very well. This finding corresponds to the conclusion of the previous study [32], that the discharge operated in tungsten cathodes provides pure hydrogen plasma. However, in stainless steel, due to the presence of sputtered material, d_{cf} is additionally compressed (see figure 3), therefore the recorded luminosity does not show the real d_{cf} value (yellow arrows). Of course, when the amount of sputtered material is not so dominant (figure 9 (a)) the d_{cf} values, both measured and estimated from the images, are more similar than in the case where the cathode fall is seriously affected by sputtering (figure 9 (b)). We can conclude therefore, that in the case of pure hydrogen plasma, the luminosity of the visible spectral range can provide a good estimation of the cathode fall length [46].

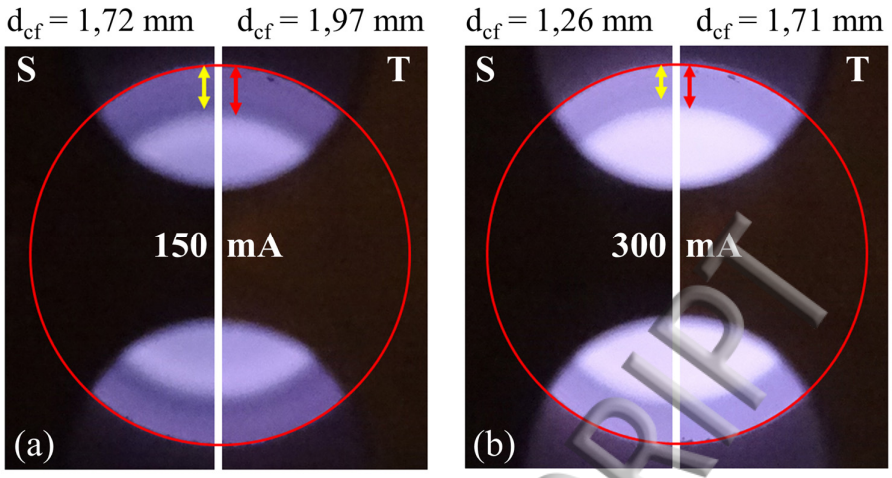

Figure 9: Comparison of luminosity images for 400 Pa for (a) 150 mA and (b) 300 mA. The left side corresponds to stainless steel and the right side to tungsten cathode. The red arrows indicates the cathode fall length (d_{cf}) in tungsten, and the yellow arrows d_{cf} in stainless steel obtained from figure 3.

5. Summary

In this work, we present high resolution local electric field strength measurements conducted in a hydrogen hollow cathode discharge (HCD) to determine cathode fall characteristics for stainless steel cathodes and to compare the new results with those recently obtained for tungsten. The excellent long and short term stability as well as the high reproducibility of discharge parameters, required for such a comparison, is provided by the design and the versatility of our HCD, because cathodes of different diameters and materials can be inserted.

The E-field determination is based in the splitting and shifting of the 2S level of hydrogen caused by the Stark effect. Two counter-propagating circularly polarized laser beams provide Doppler-free two-photon absorption measurements. The subsequent photo-ionization due to the absorption of a third photon caused the optogalvanic signal. The E-field values are obtained from the frequency splitting of the Stark components: $2P^{1/2}$ and $2P^{3/2}$. The laser radiation of 243 nm needed for the measurements is generated by a UV laser spectrometer that delivers single longitudinal mode pulses with 2.5 ns temporal duration and 300 MHz bandwidth. The overlap of the two laser beams provides an exceptional high spatial resolution: 100 µm in diameter and 10 mm in length. This measurement volume is aligned in the centre and parallel to the cathode surface.

The new E-field measurements have been performed in a wide range of pressures (from 400 to 900 Pa) and currents (from 50 to 300 mA), in two stainless steel cathodes with 10 and15 mm inner diameter. Measurements obtained for the same current densities for both diameters revealed - in agreement with tungsten cathode - that the cathode fall characteristics does not depend on discharge geometry.

When comparing different cathode materials, the perturbation of the discharge due to sputtering reveals itself as the main cause of the differences in the cathode fall. To analyse this influence we study different parameters: the maximum E-field at the cathode surface, the length of the cathode region, and the entire cathode fall voltage obtained from the integral of the E-field variation. All these results confirm that the hollow cathode discharge with tungsten cathodes serve very well as reference of pure hydrogen plasma, and sputtering is negligible in a wide range of discharge conditions. However, for stainless steel due to sputtered iron present in the proximity of the cathode surface, the discharge does

not provide pure hydrogen plasma. In this case, the perturbation of the cathode fall due to sputtering increases with lower pressure and increasing current. Furthermore, we can concluded, that sputtering of stainless steel cathodes used for hydrogen discharges is nearly negligible for normalized current densities remarkably smaller than e.g. 10^{-4} A/Torr^{2}cm^2.

End on taken images of the discharge luminosity allowed for another complementary comparison. For all discharge conditions, the luminosities are almost the same for stainless and tungsten and show the cathode fall extension as a well pronounced dark zone. The radial length of this dark zone fits perfectly with the lengths of the cathode fall region d_{cf} obtained for tungsten from the precision measurements, but does not correspond to d_{cf} obtained for stainless steel cathodes. This is referred to the presence of sputtered material in the cathode fall, which does not show up in the luminosity still dominated by the visible radiation of the hydrogen discharge, and leads to the interesting conclusion, that images of the discharge luminosity of pure hydrogen may provide in good approximation the cathode fall lengths.

In a previous paper we conclude that E-field measurements conducted on the HCD with tungsten cathode serve as reference and can be used to test one dimensional modelling of cathode fall dynamics. Nevertheless, in the case of stainless steel cathodes modelling has to account additionally for a laminar hydrogen gas flow parallel to the cathode surface present in our HCD. Therefore the incorporation of the sputtered material is more complex and makes direct comparison with other discharge geometries more difficult. The experimental technique presented in this study can furthermore be applied to determine cathode fall characteristics for low pressure discharge operated with deuterium, i.e. to study the impact on the discharge dynamic by varying the atomic mass of the hydrogen isotopes by a factor of two.

Acknowledgments

The authors thank DGICYT (Ministerio de Economía y Competitividad) for the project ENE2012-35902, FEDER funds and the grants BES-2013-063248 and EEBB-I-17-12659 given to V. González-Fernández. The authors thank A. Martín and S. González for the technological support, J. L. Nieto for the informatics help, E. M. Domingo for the administrative work and A. Steiger and L. M. Fuentes for the scientific discussions.

6. References

[1] K. Muraoka and M. Maeda. "Laser-aided diagnostics of plasmas and gases", IoP Publishing, Bristol (2001)

[2] J. A. Bittencourt. "Fundamentals of plasma physics", Springer Science & Bussines Media (2013)

[3] Y. P. Raizer and J. E. Allen "Gas discharge physics", Springer, Berlin (1997)

[4] I. Adamovich et al., J. Phys. D 50(32), 323001 (2017)

[5] S. Samukawa et al., J. Phys. D, 45(25), 253001 (2012)

[6] G. Lj. Majstorović, N. M. Šišović and N. Konjević, Phys. Plasmas, 14(4), 043504 (2007)

[7] G. Lj. Majstorović, N. M Šišović,and N. Konjević, Plasma Sources Sci. Technol., 16(4), 750 (2007)

[8] P. Böhm, M. Kettlitz, R. Brandenburg, H. Höft and U. Czarnetzki, Plasma Sources Sci. Technol., 25(5), 054002 (2016)

[9] J. Schulze, Z. Donkó, B. Heil, D. Luggenhölscher, T. Mussenbrock, R. Brinkmann and U. Czarnetzki, J. Phys. D, 41(10), 105214 (2008)

[10] A. Sobota, O. Guaitella and E. Garcia-Caurel, J. Phys. D, 46(37), 372001 (2013)

[11] U. Czarnetzki, D. Luggenhölscher and H. Döbele, Phys. Rev. Lett. 81(21), 4592 (1998)

[12] T. Kampschulte, J. Schulze, D. Luggenhölscher, M. Bowden and U. Czarnetzki, New J. Phys., 9(1), 18 (2007)

[13] J. Lawler and D. Doughty, Adv. At. Mol. Opt. Phys., 34, 171-206 (1994)

[14] K. Greenberg and G. Hebner, App. Phys. Lett., 63(24), 3282-3284 (1993)

[15] V. Gavrilenko, H. Kim, T. Ikutake, J. Kim, Y. Choi, M. Bowden and K. Muraoka, Phys.Rev. E, 62(5), 7201 (2000)

[16] J. Booth, M. Fadlallah, J. Derouard and N. Sadeghi, App. Phys. Lett., 65(7), 819 (1994)

[17] V. Gavrilenko, Instruments and Experimental Techniques, 49(2), 149 (2006)

[18] G. Hebner, K. Greenberg and M. Riley, J. App. Phys., 76(7), 4036 (1994)

[19] M. Alberta, H. Debontride, J. Derouard and N. Sadeghi, Journal de Physique III, 3(1), 105 (1993)

[20] Y. Choi, M. Bowden and K. Muraoka, App. Phys. Lett., 69(10), 1361 (1996)

[21] R. A. Gottscho, Phys.Rev. E, 36(5), 2233 (1987)

[22] Dj. Spasojević, S. Mijin, N. M. Šišović, and N. Konjević, J. App. Phys. 119(5) 053301 (2016

[23] N. Cvetanović, B. Obradović and M. Kuraica, J. App. Phys., 109(1), 013311 (2011)

[24] N. Šišović, G. Lj. Majstorović and N. Konjević, Eur. Phys. J. D, 32(3), 347 (2005)

[25] I. Videnović, N. Konjević and M. Kuraica, Spectrochim. Acta, Part B, 51(13), 1707 (1996)

[26] N. Baguer and A. Bogaerts, J. App. Phys., 98(3), 033303 (2005)

[27] B. N. Chapman, "Glow discharge processes", Wiley, (1980)

[28] N. Baguer, A. Bogaerts and R. Gijbels, J. App. Phys., 94(4), 2212 (2003)

[29] M. I. de la Rosa, C. Pérez, K. Grützmacher, A. Gonzalo and A. Steiger, Plasma Sources Sci. Technol., 15(1), 105 (2006)

[30] M. I. de la Rosa, C. Pérez, K. Grützmacher and L. M. Fuentes, Plasma Sources Sci. Technol., 18, 015012 (2008)

[31] C. Pérez, M. I. de la Rosa and K. Grützmacher, Eur. Phys. J. D, 56(3), 369 (2010)

[32] V. Gonzalez-Fernandez, K. Grützmacher, A. Steiger, C. Pérez and M. I. de la Rosa, Plasma Sources Sci. Technol., 26(10), 105004 (2017)

[33] V. Gonzalez-Fernandez, K. Grützmacher, C. Pérez and M. I. de la Rosa, Journal ol Instrumentation, 12(11), C11029 (2017)

[34] M. Garcia-Lechuga, L. M. Fuentes, K. Grützmacher, C. Pérez and M. I. de la Rosa, J. App. Phys., 116(13), 133103 (2014)

[35] A. Güntherschulze, Z. Phys., 59(7-8), 433 (1930)

[36] A. Güntherschulze, Z. Phys., 49(7-8), 473 (1928)

[37] R. Warren, Phys. Rev., 98(6), 1650 (1955)

[38] C. Barbeau and J. Jolly, App. Phys. Lett., 58(3), 237-239 (1991)

[39] N. Cvetanović, M. Kuraica and N. Konjević, J. App. Phys., 97(3), 033302 (2005)

[40] N. Matsunami, et al., Atomic data and nuclear data tables, 31(1), 1 (1984)

[41] Z. Donkó, Plasma Sources Sci. Technol., 20(2), 024001 (2011)

[42] A. Phelps, Plasma Sources Sci. Technol., 20(4), 043001 (2011)

[43] F. Sigeneger, Z. Donko and D. Loffhagen, Eur. Phys. J. Appl. Phys., 38(2), 161 (2007)

[44] N. Baguer, A. Bogaerts, Z. Donko, R. Gijbels and N. Sadeghi J. App. Phys., 97(12), 123305 (2005)

[45] J. Van Dijk, G. M. W. Kroesen and A. Bogaerts, J. Phys. D, 42(19), 190301 (2009)

[46] Y. Fu, H. Luo, X. Zou and X. Wang, Phys. Plasmas, 22(2), 023502 (2015)

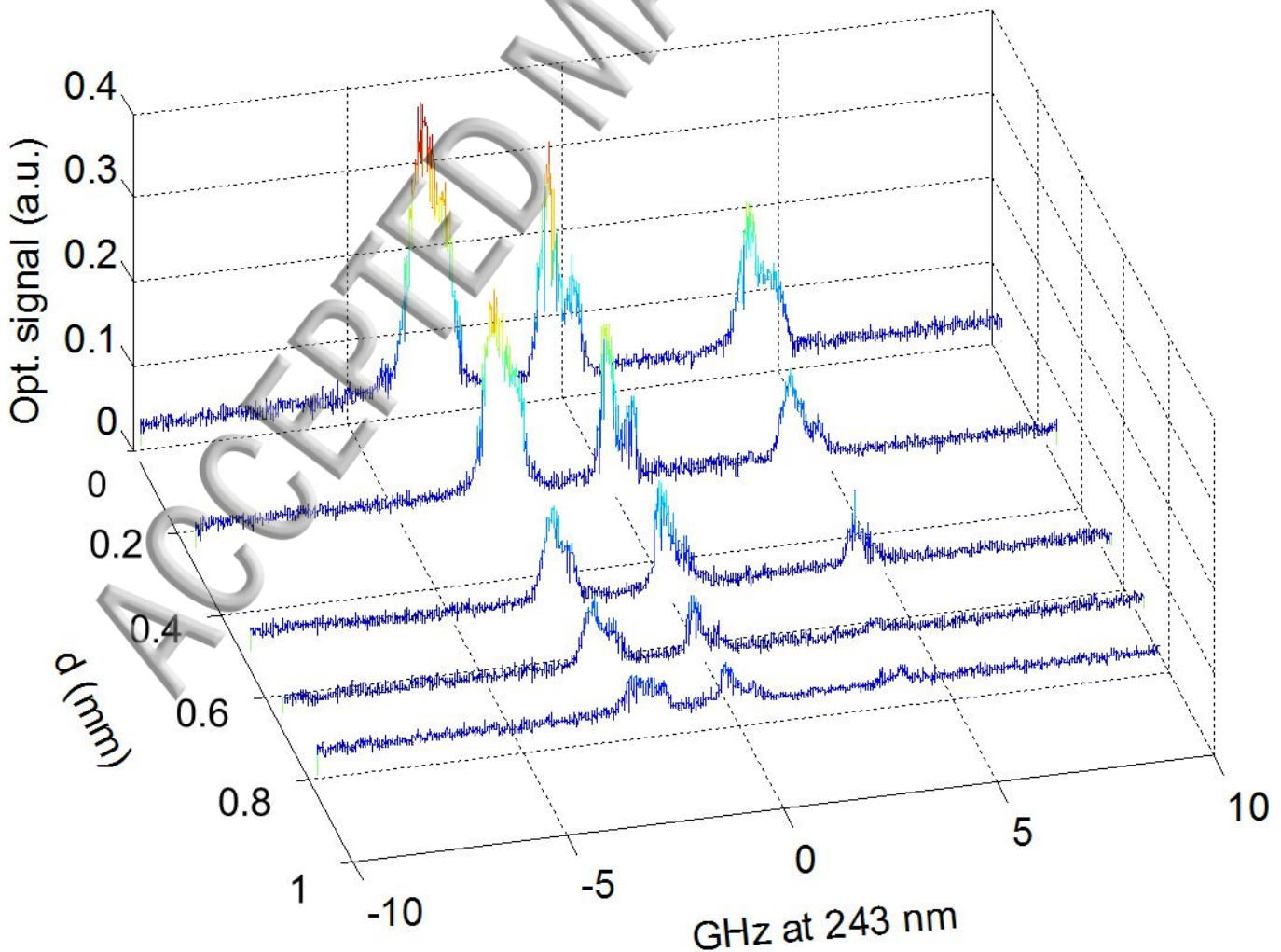
Opt. signal (a.u.)
0.4
0.3
0.2
0.1
0
0
0.2
0.4
0.6
0.8
1
(mm) ρ
-10
-5
0
5
10
GHz at 243 nm

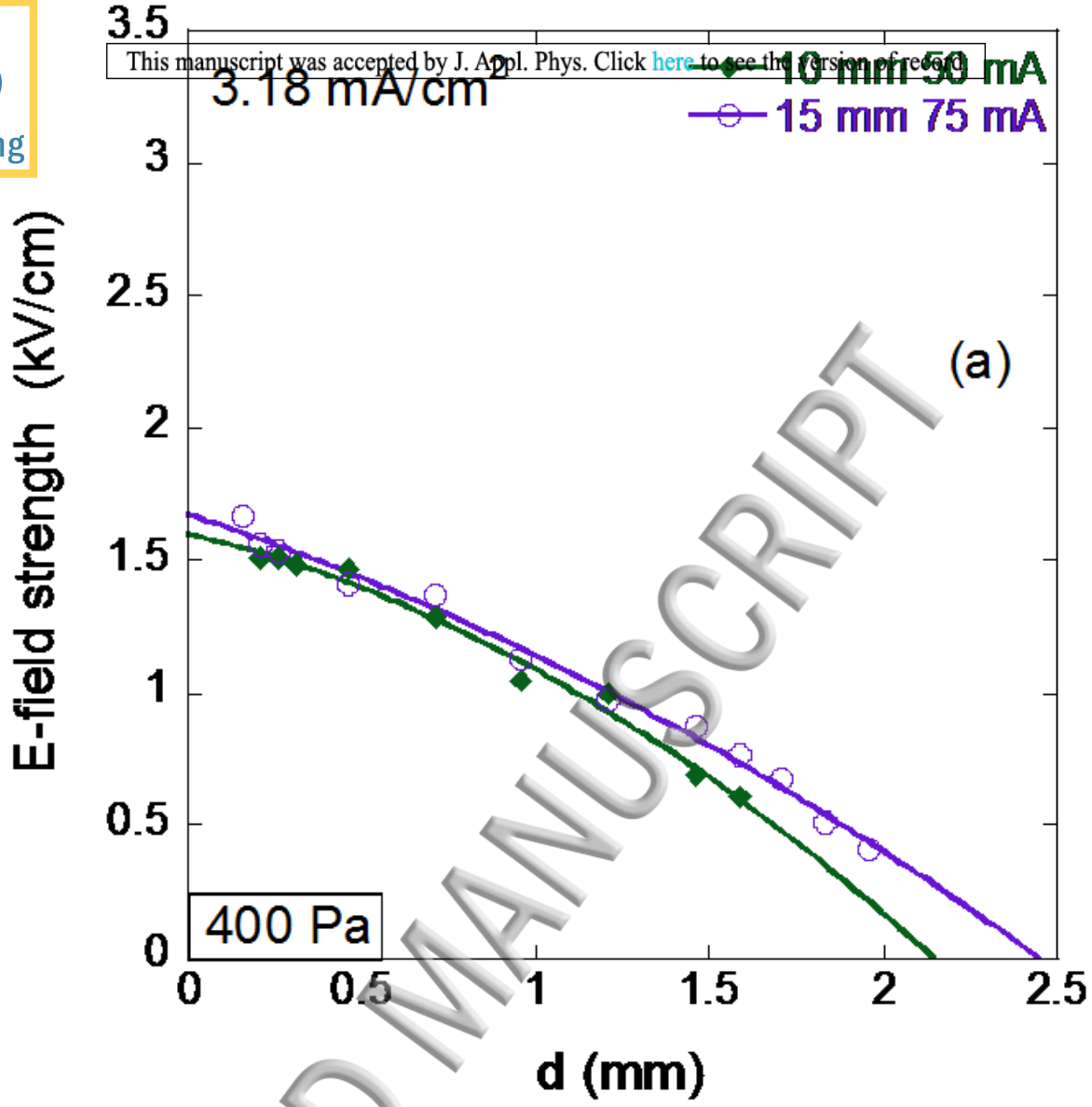

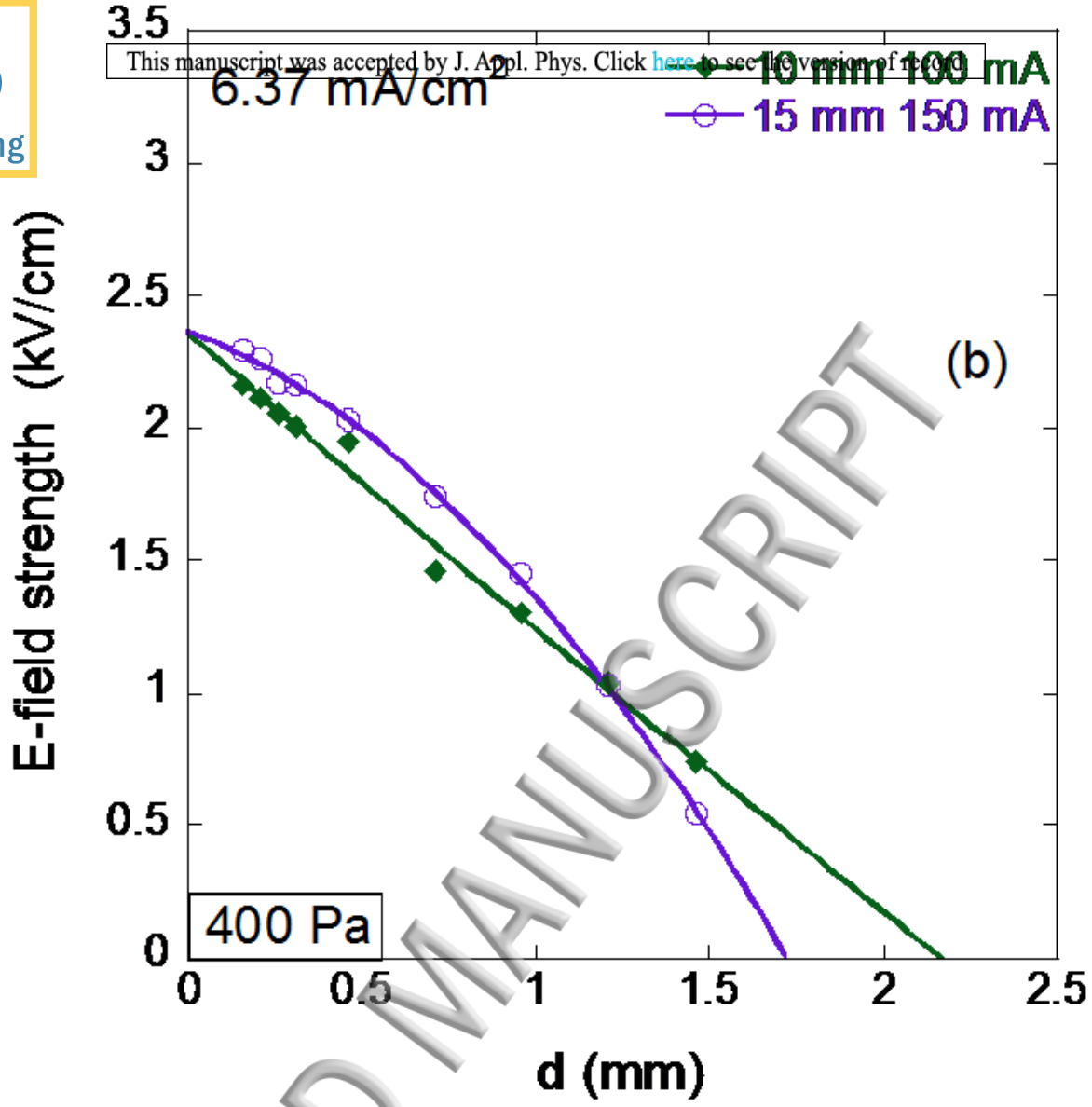

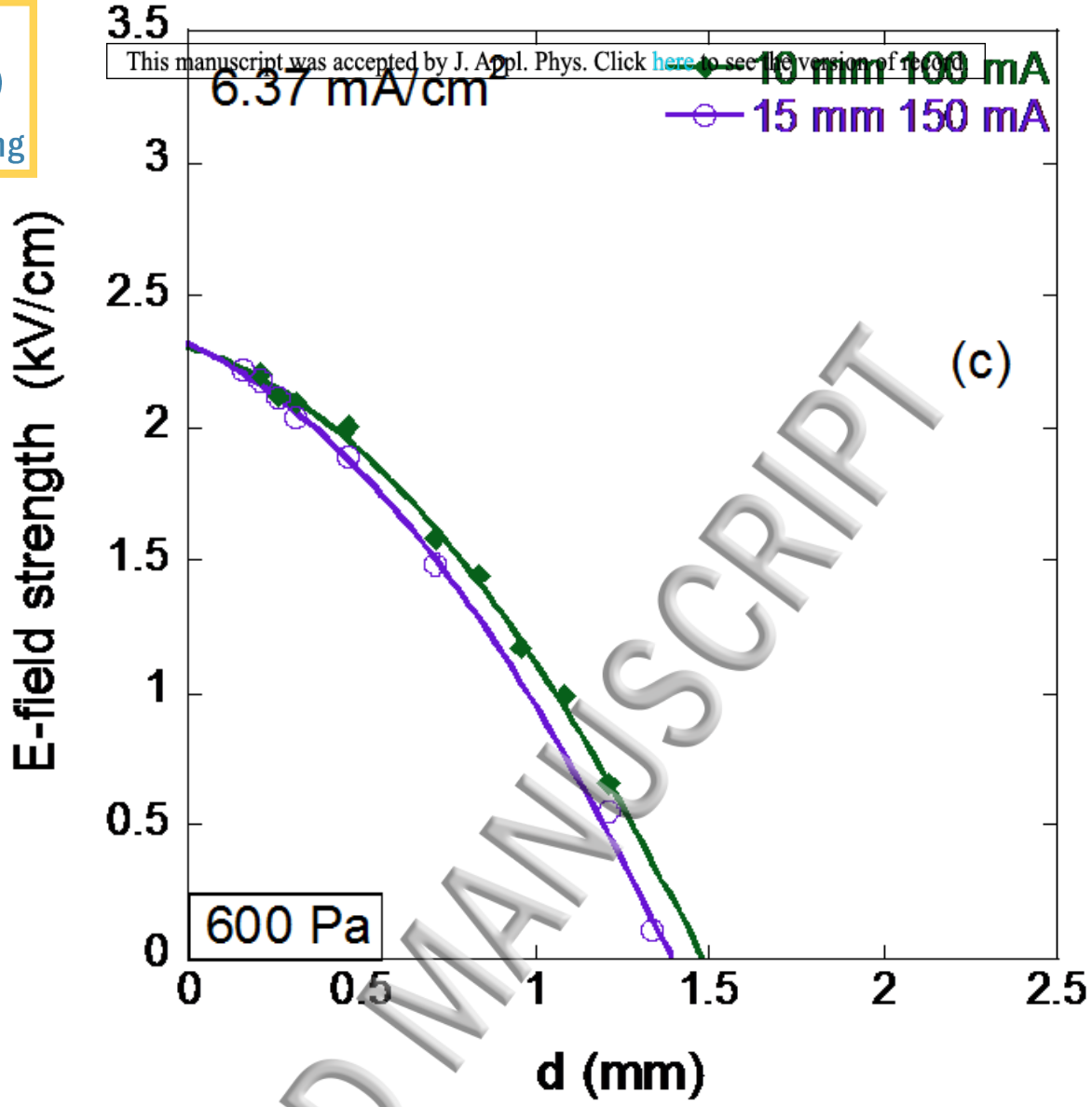

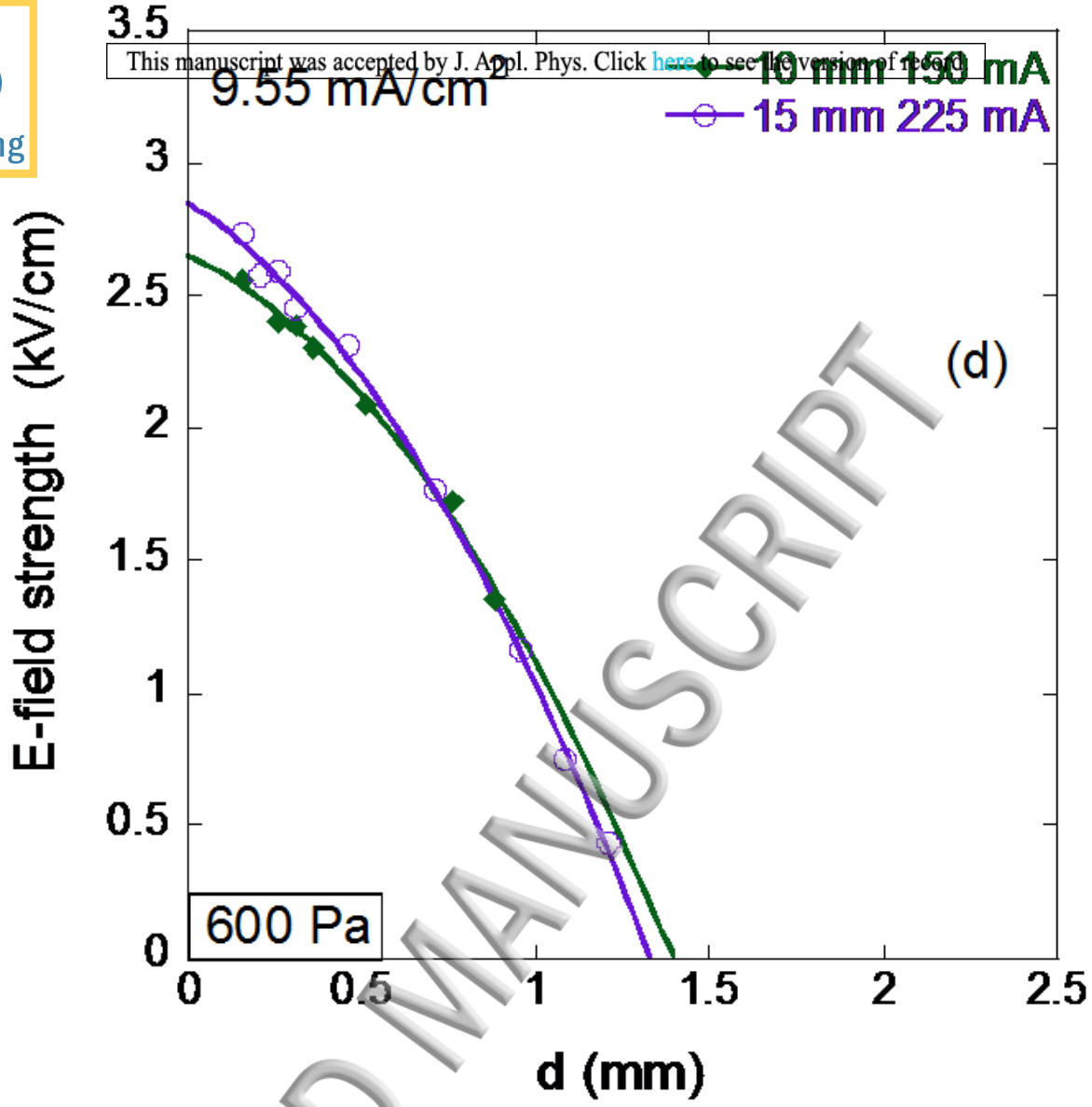

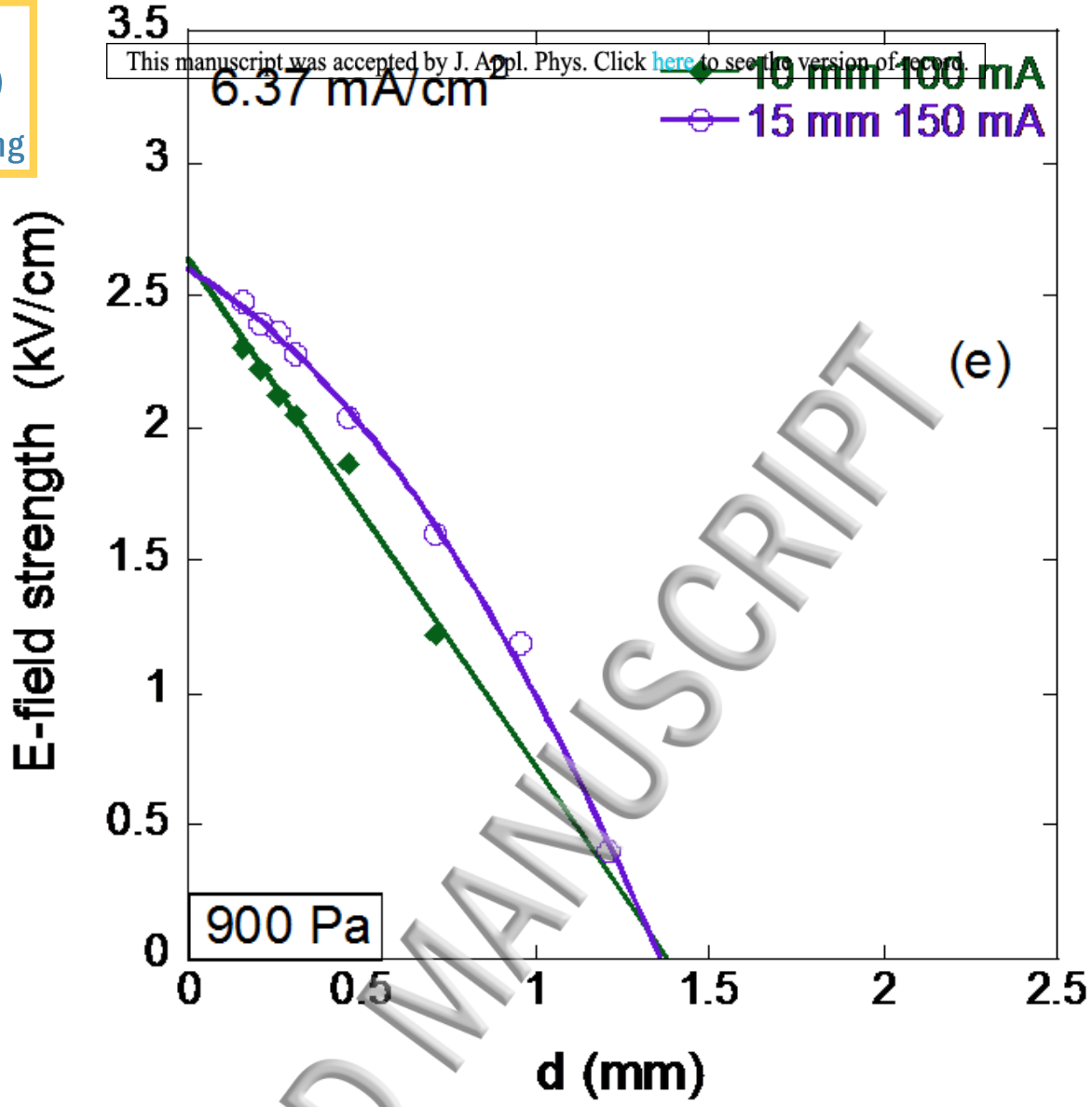

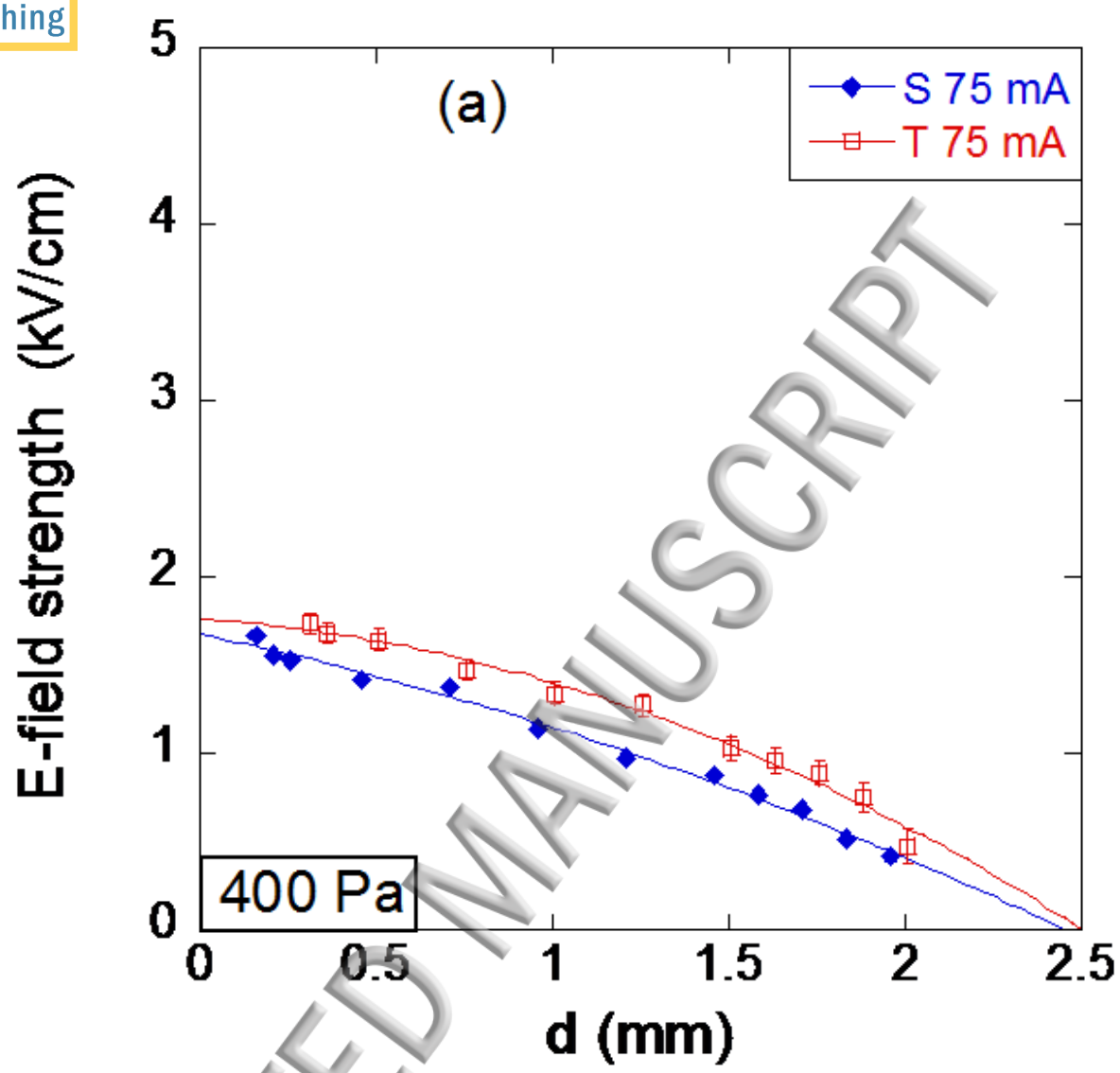

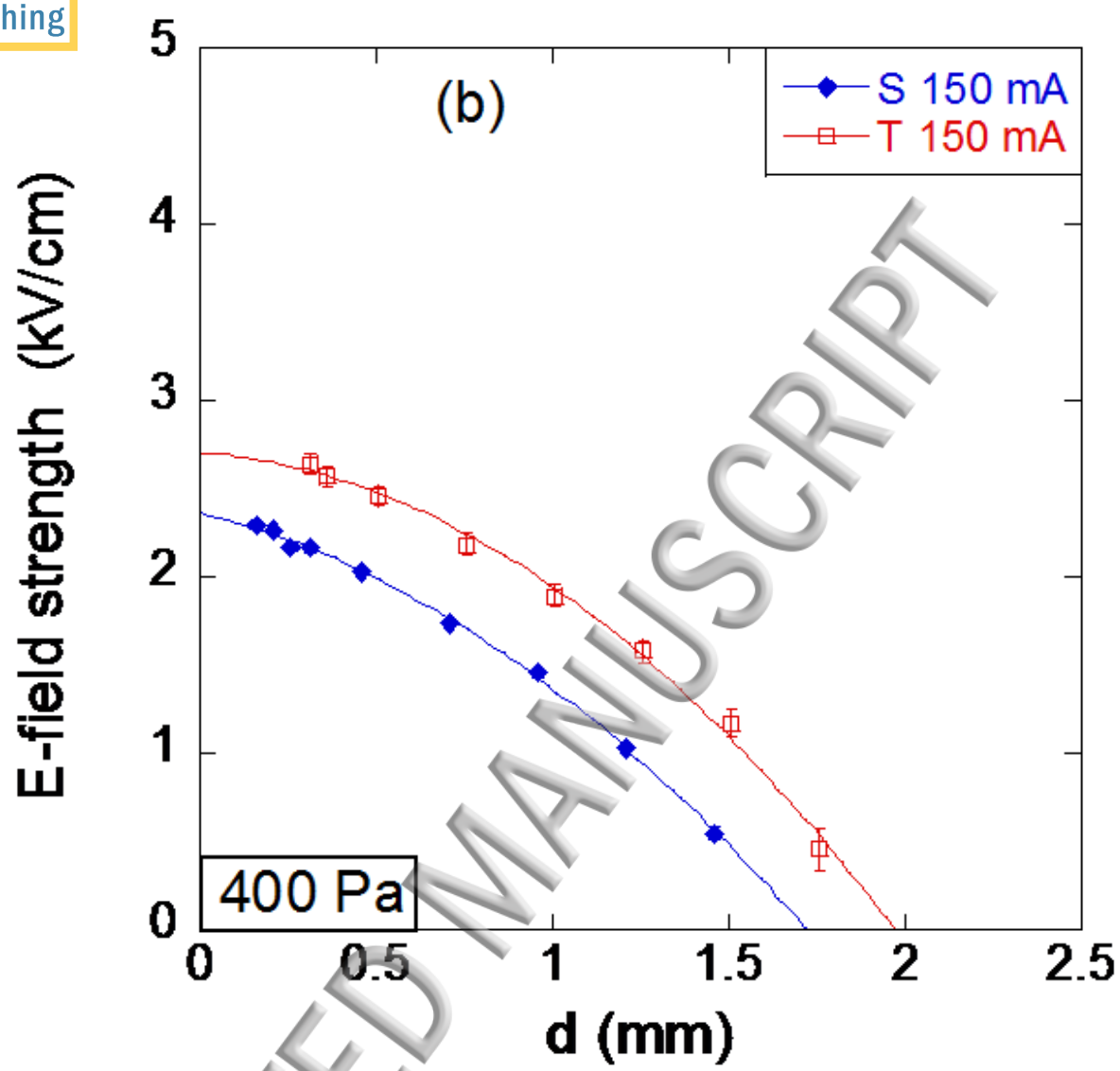

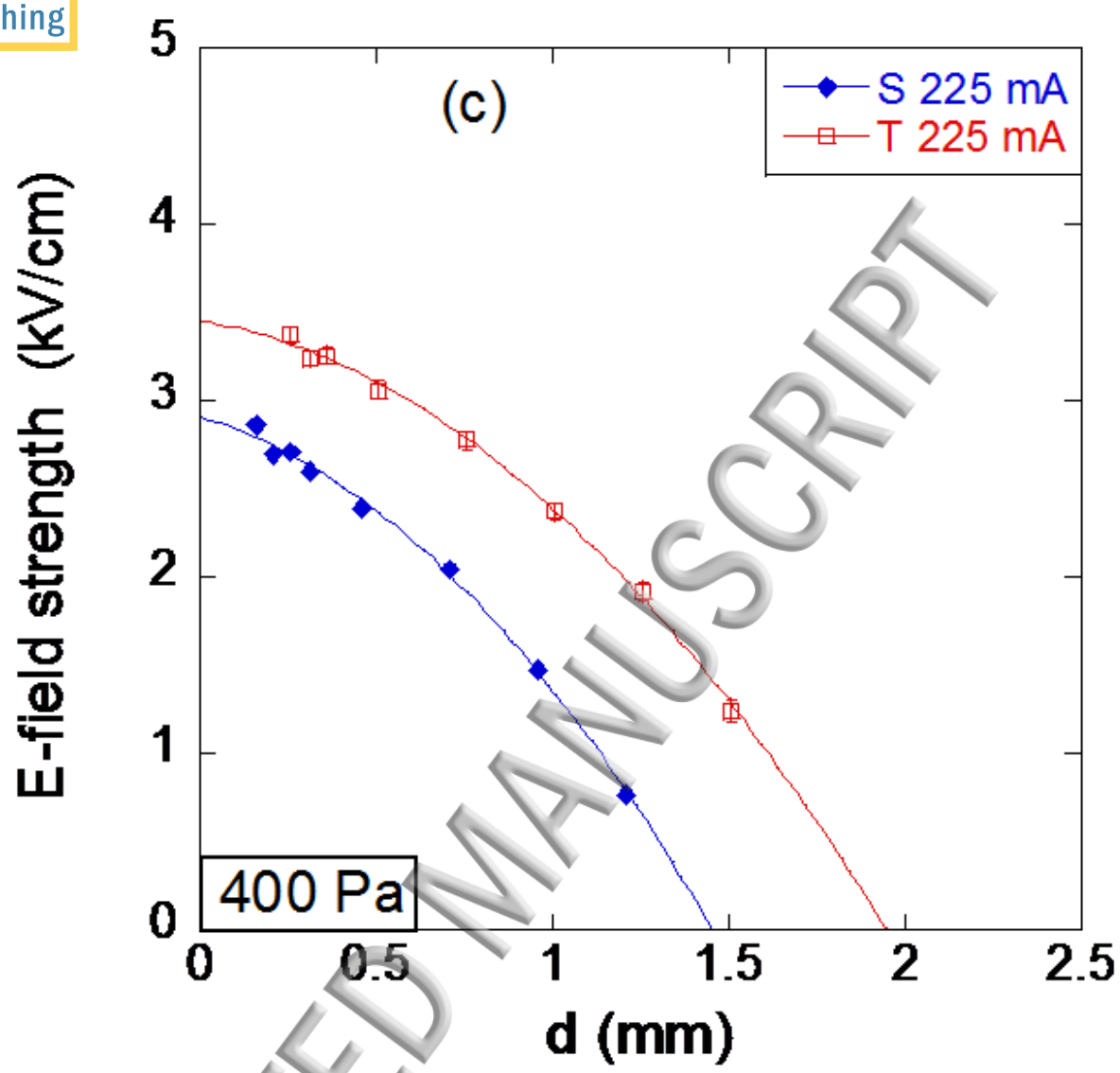

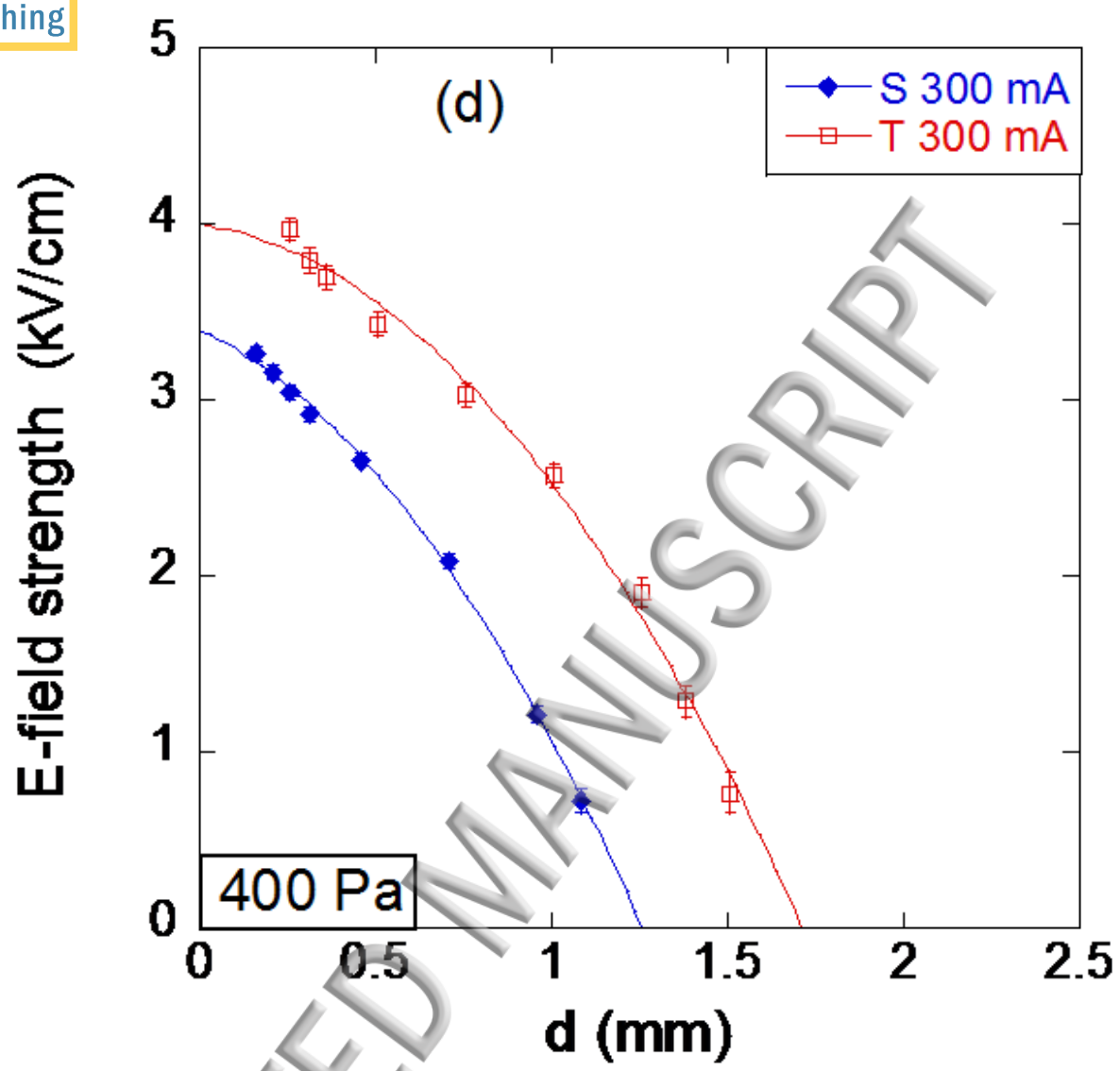

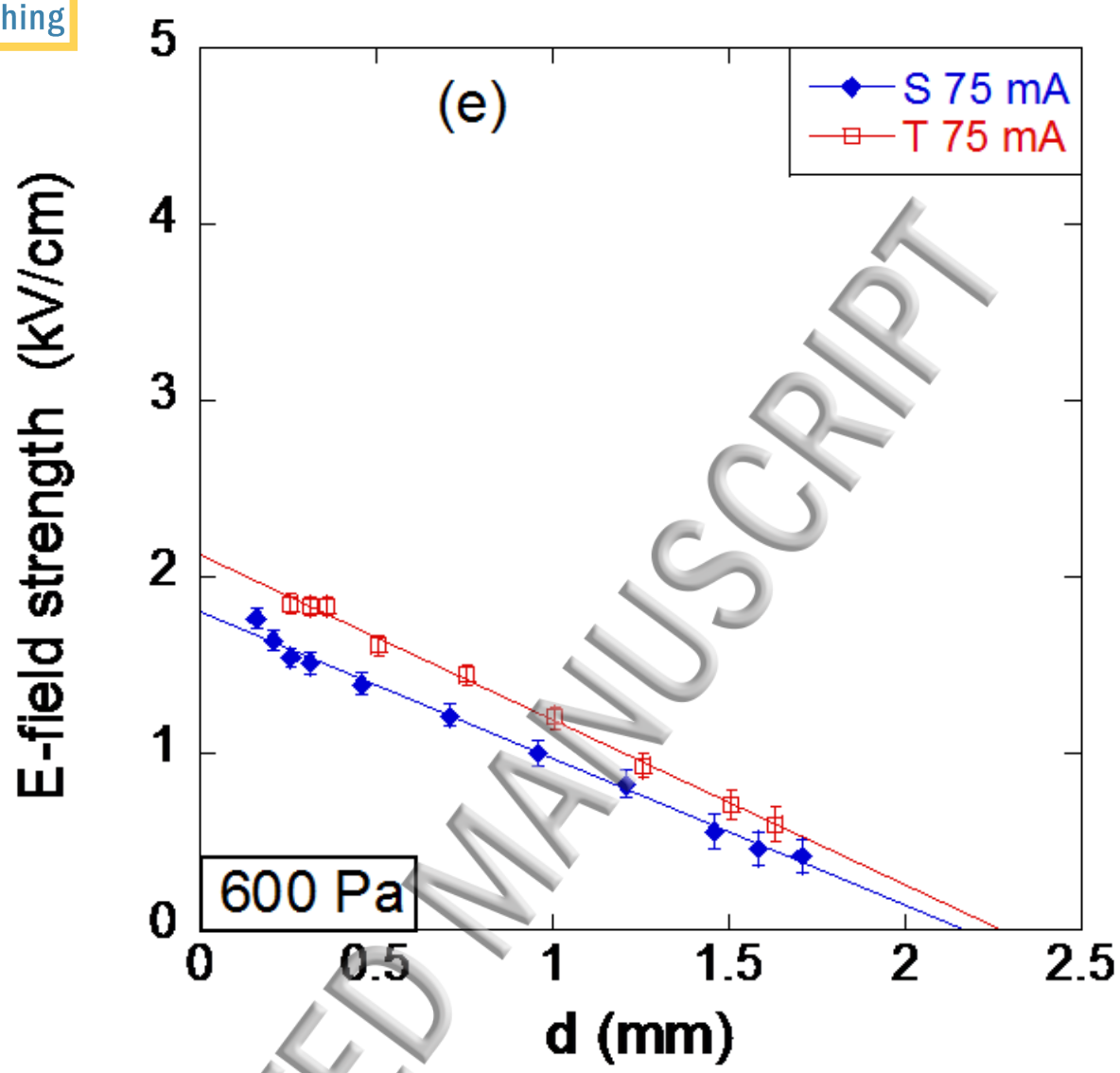

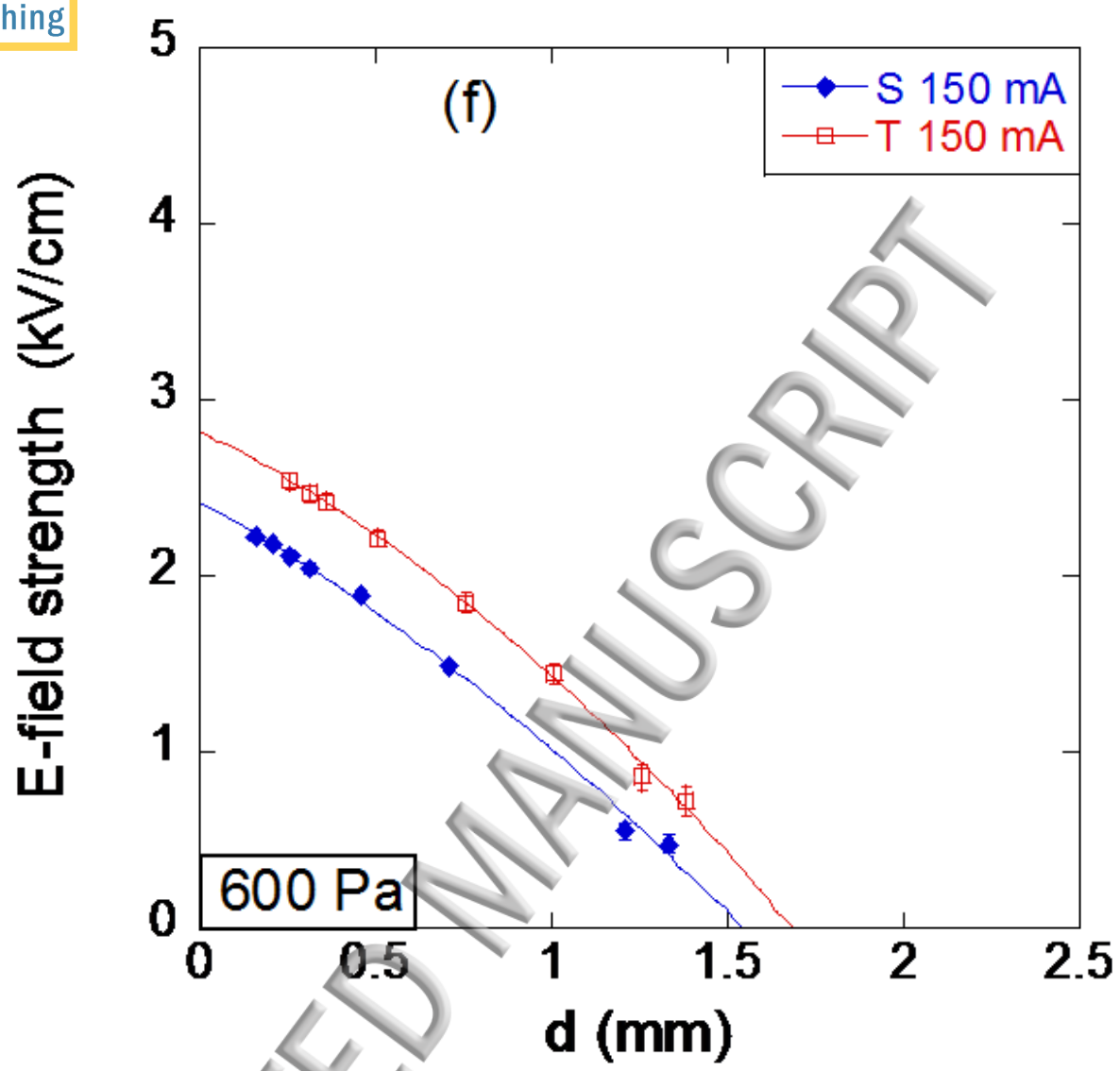

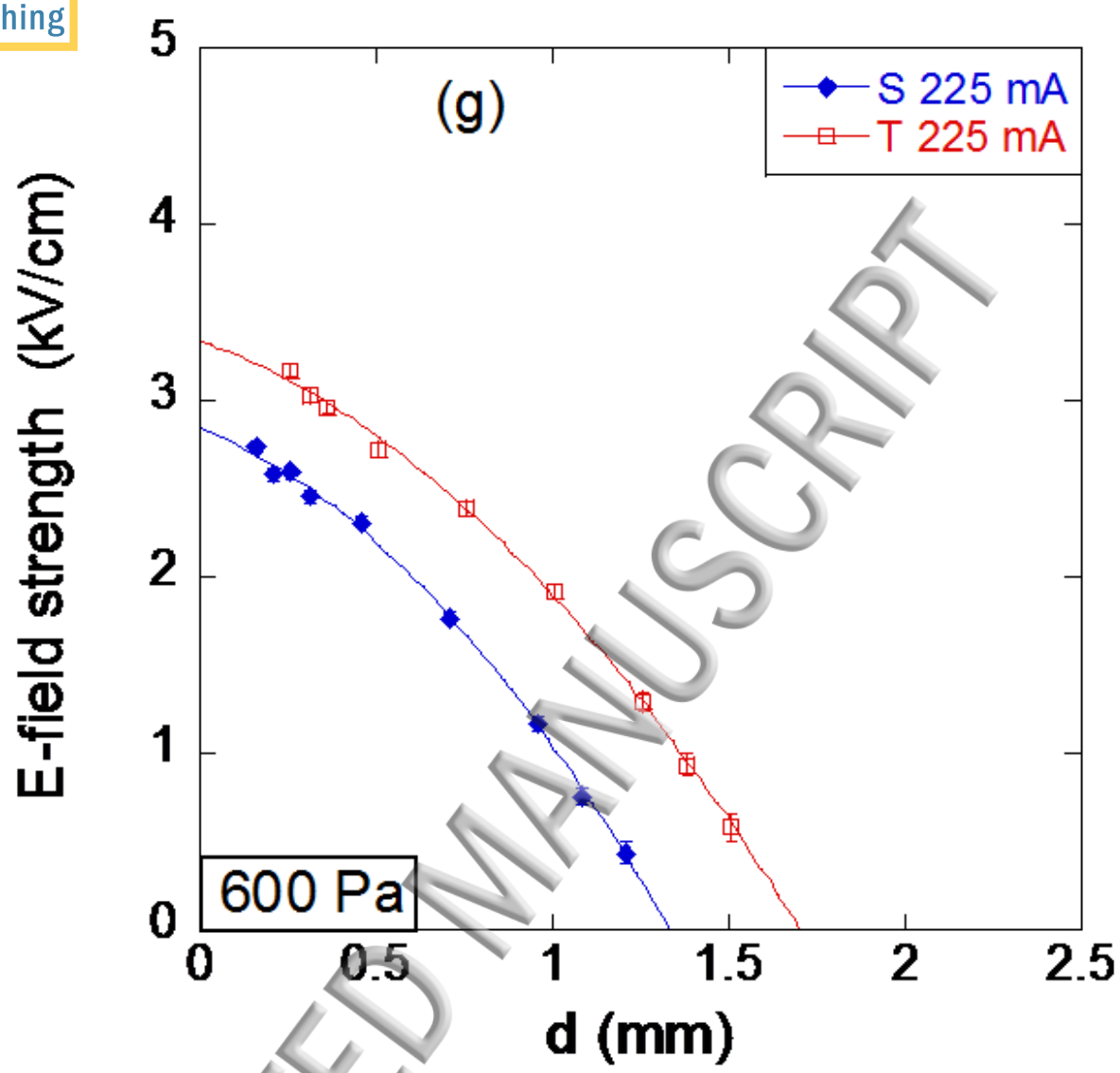

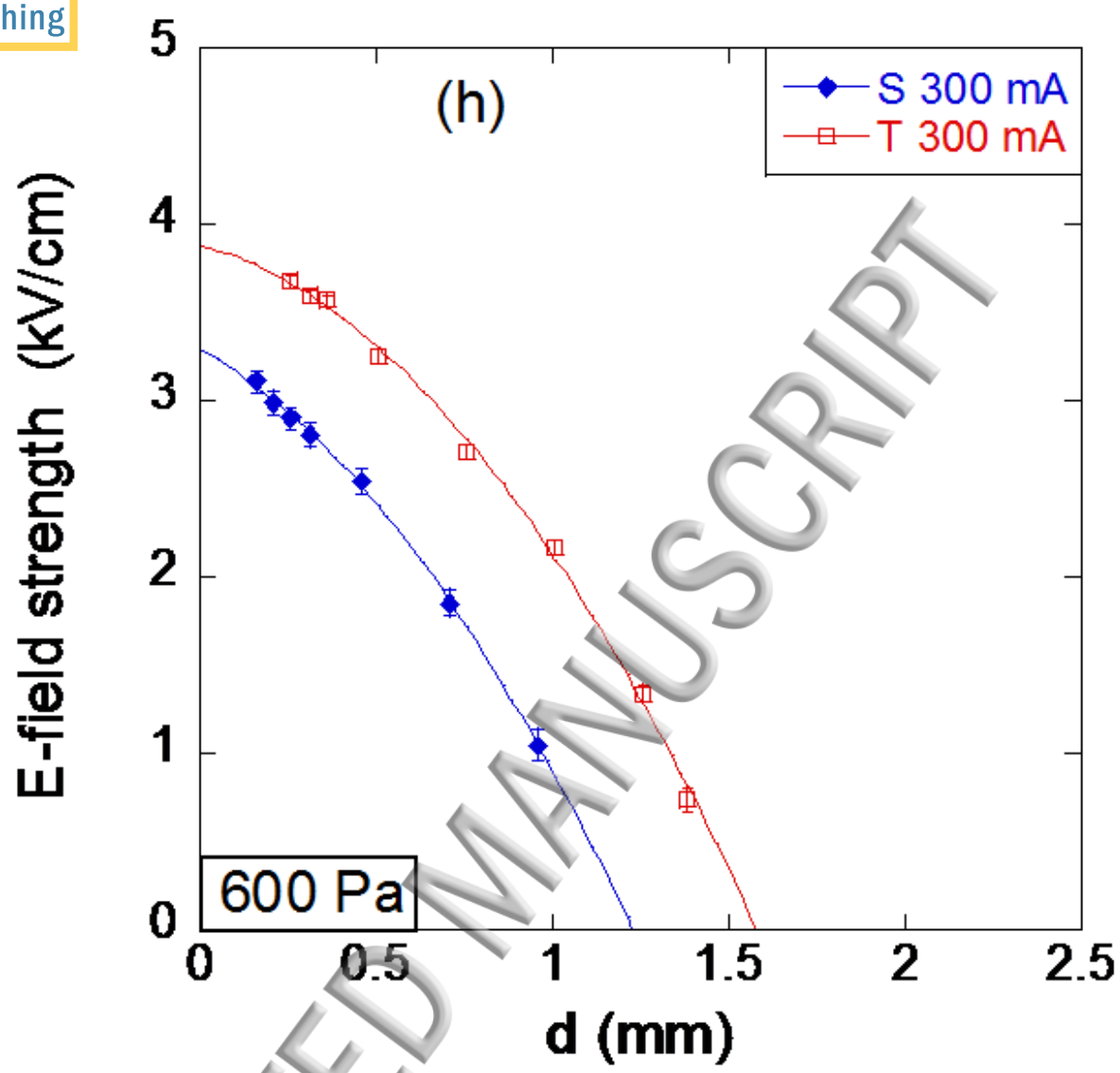

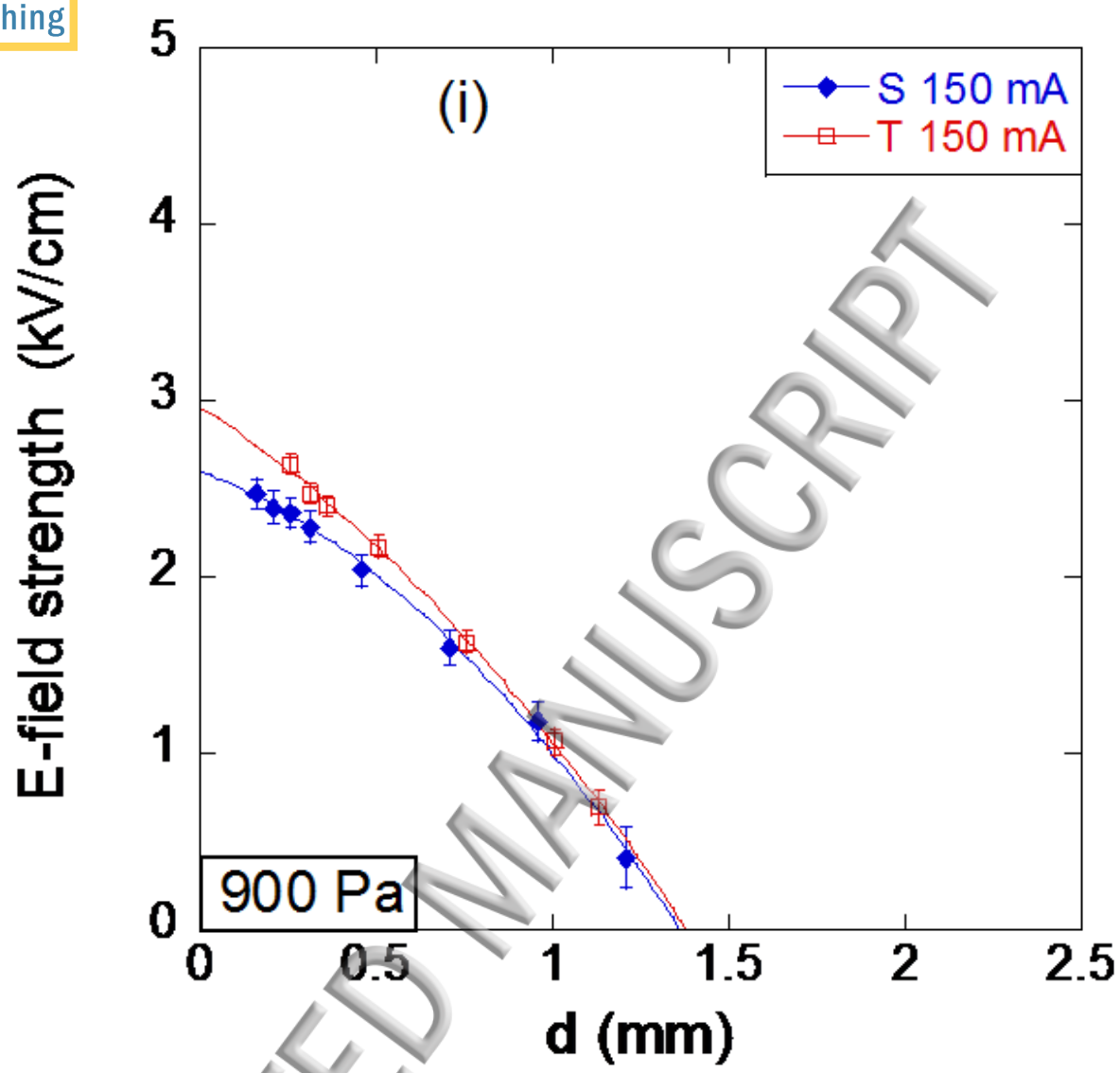

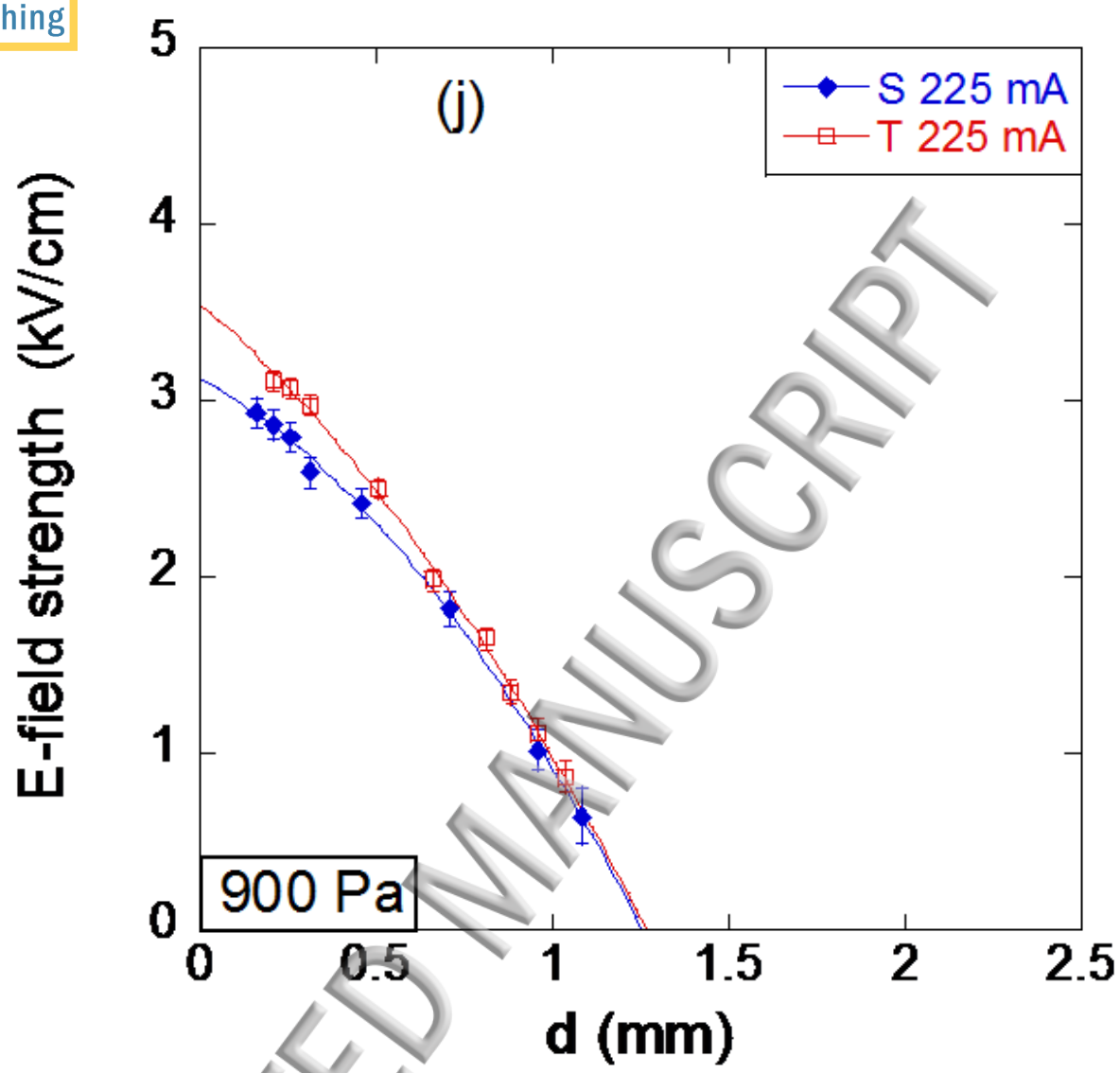

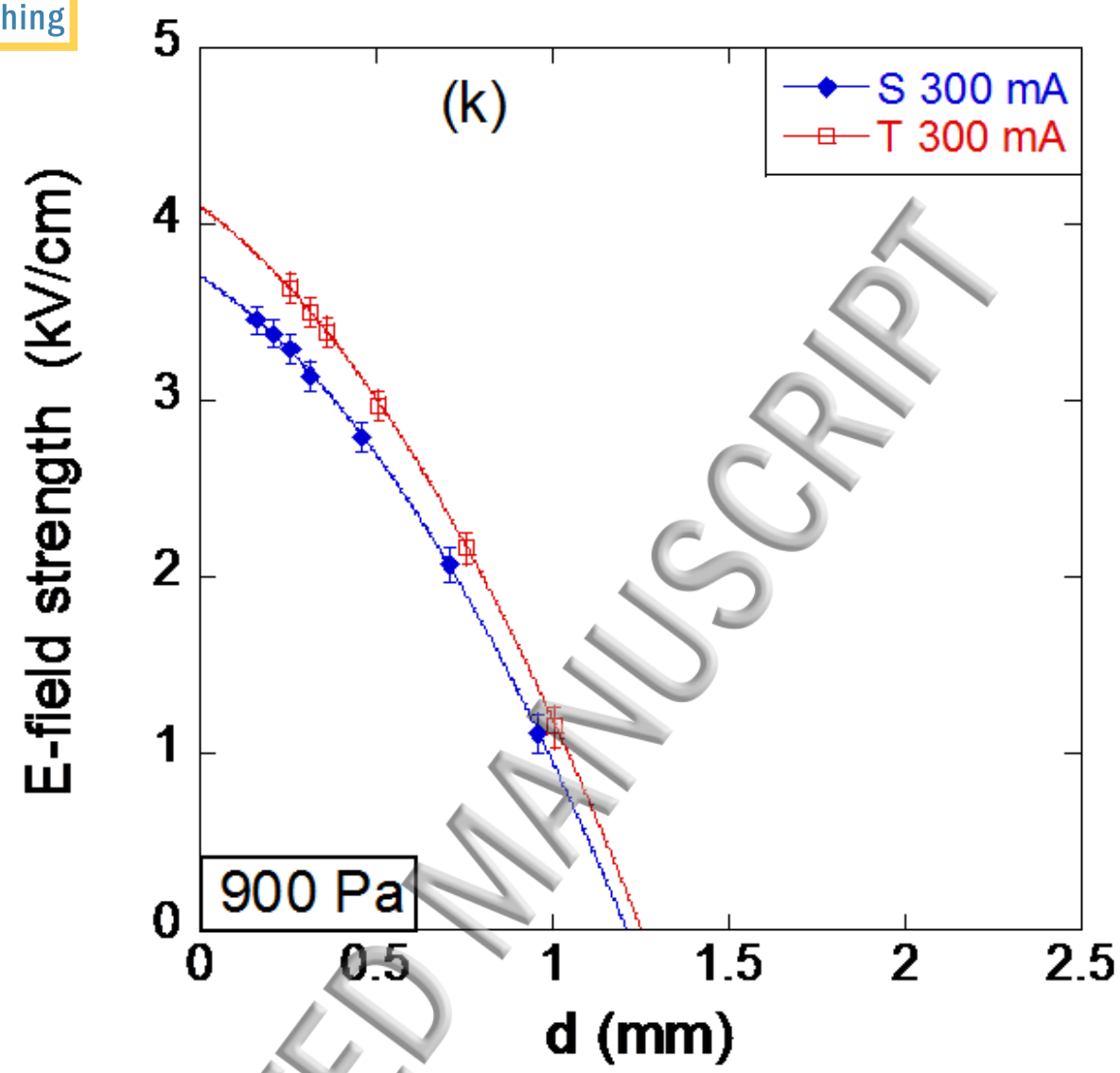

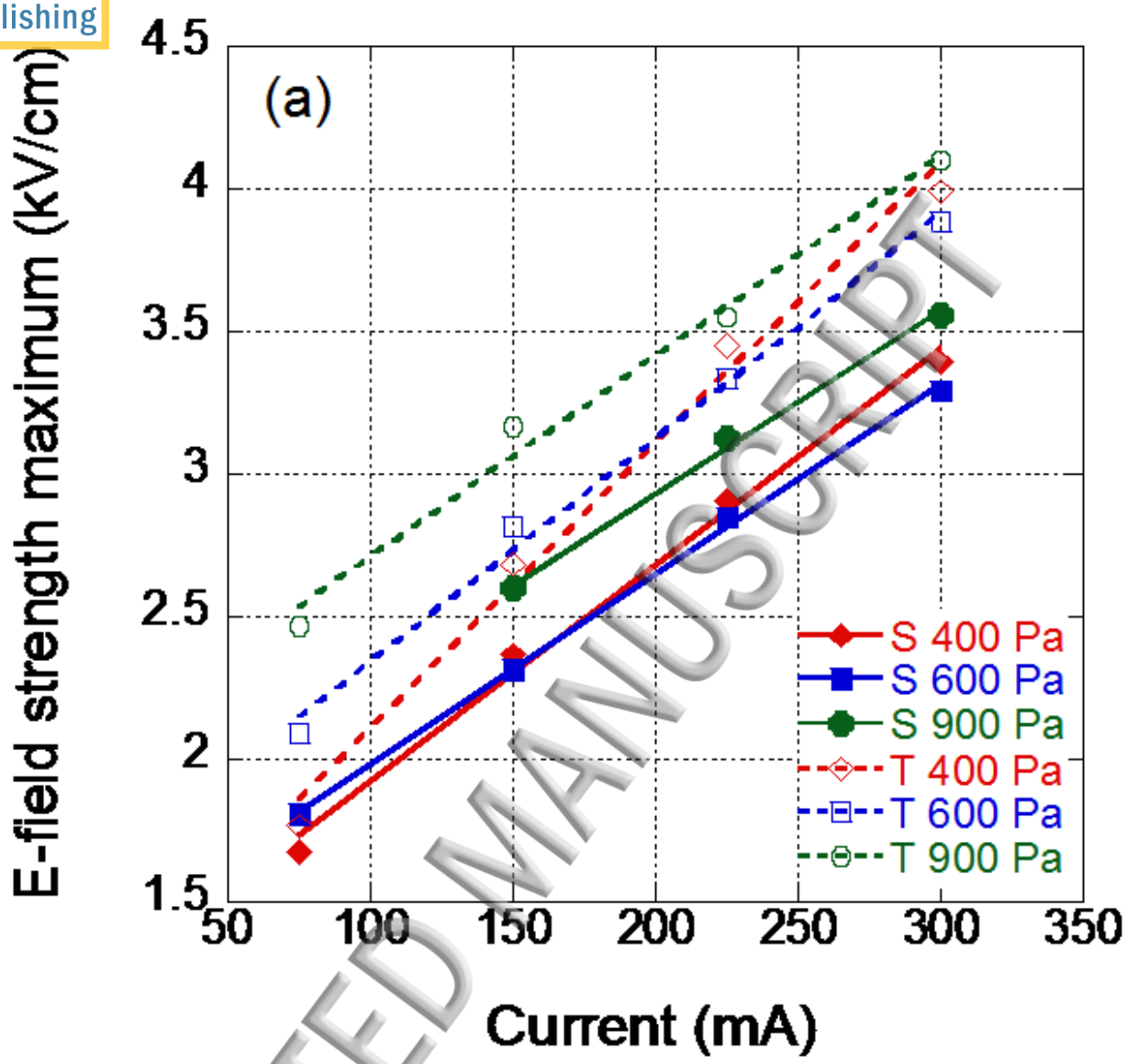

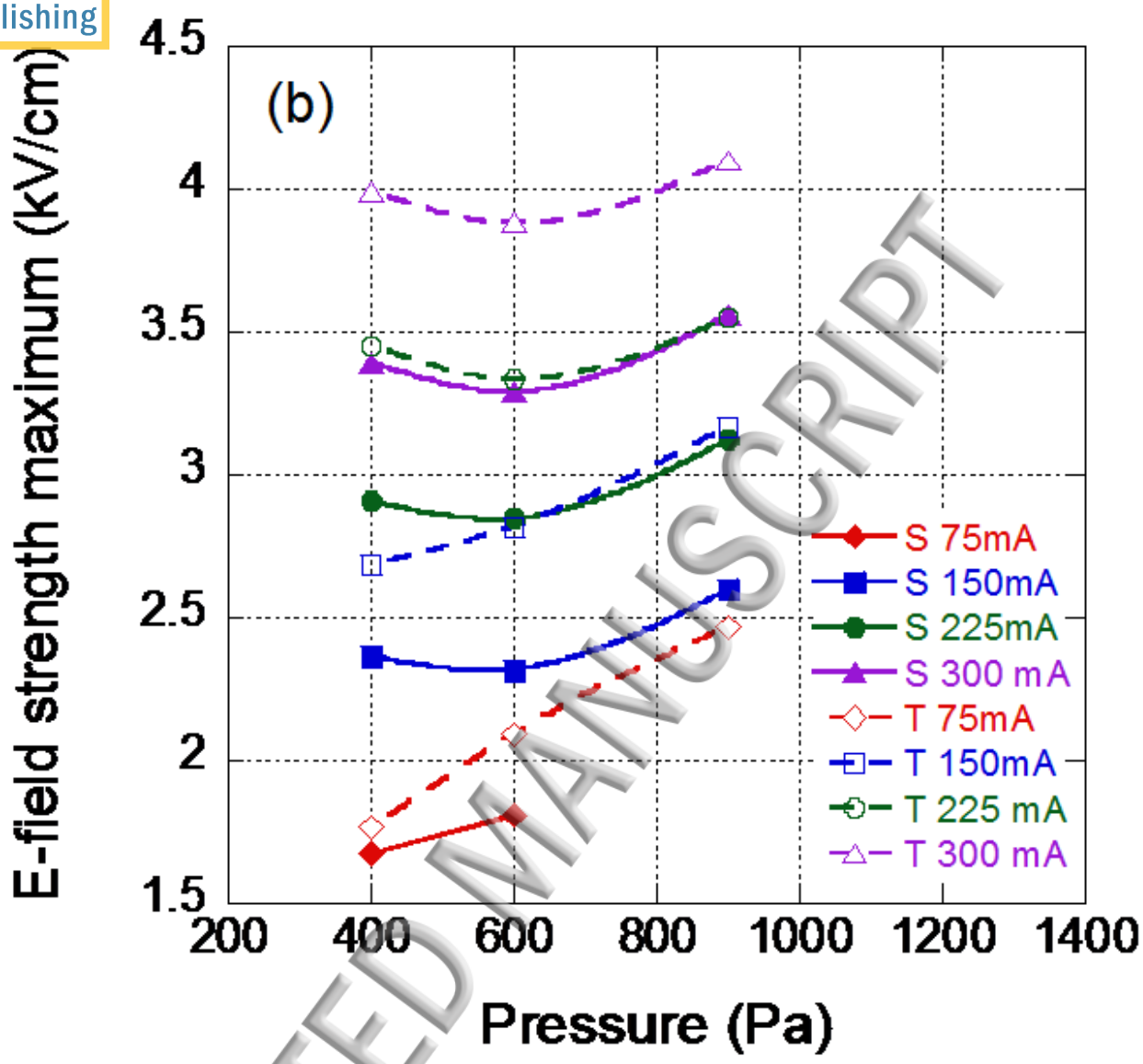

This manuscript was accepted by J. Appl. Phys. Click here to see the version of record.

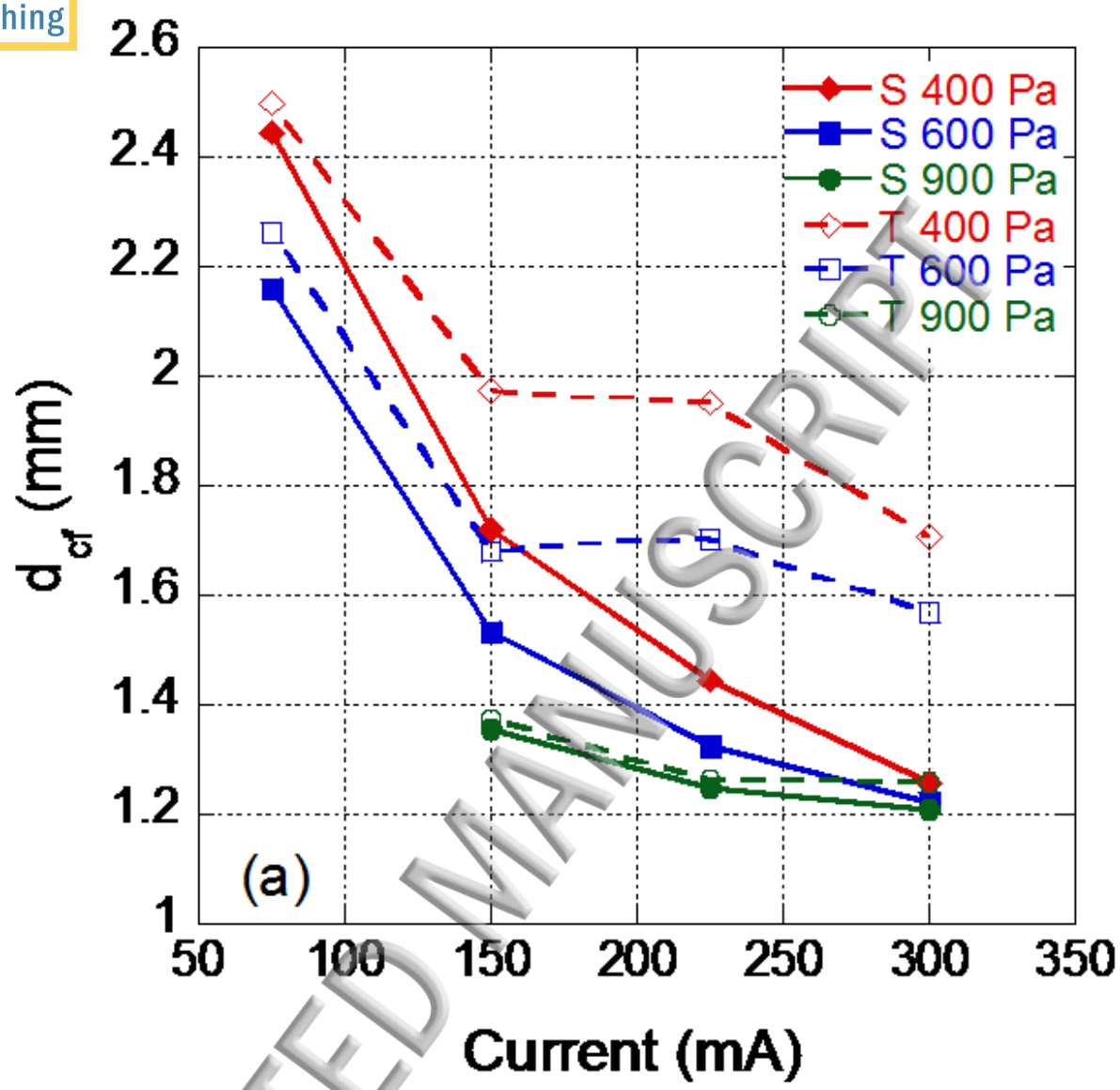

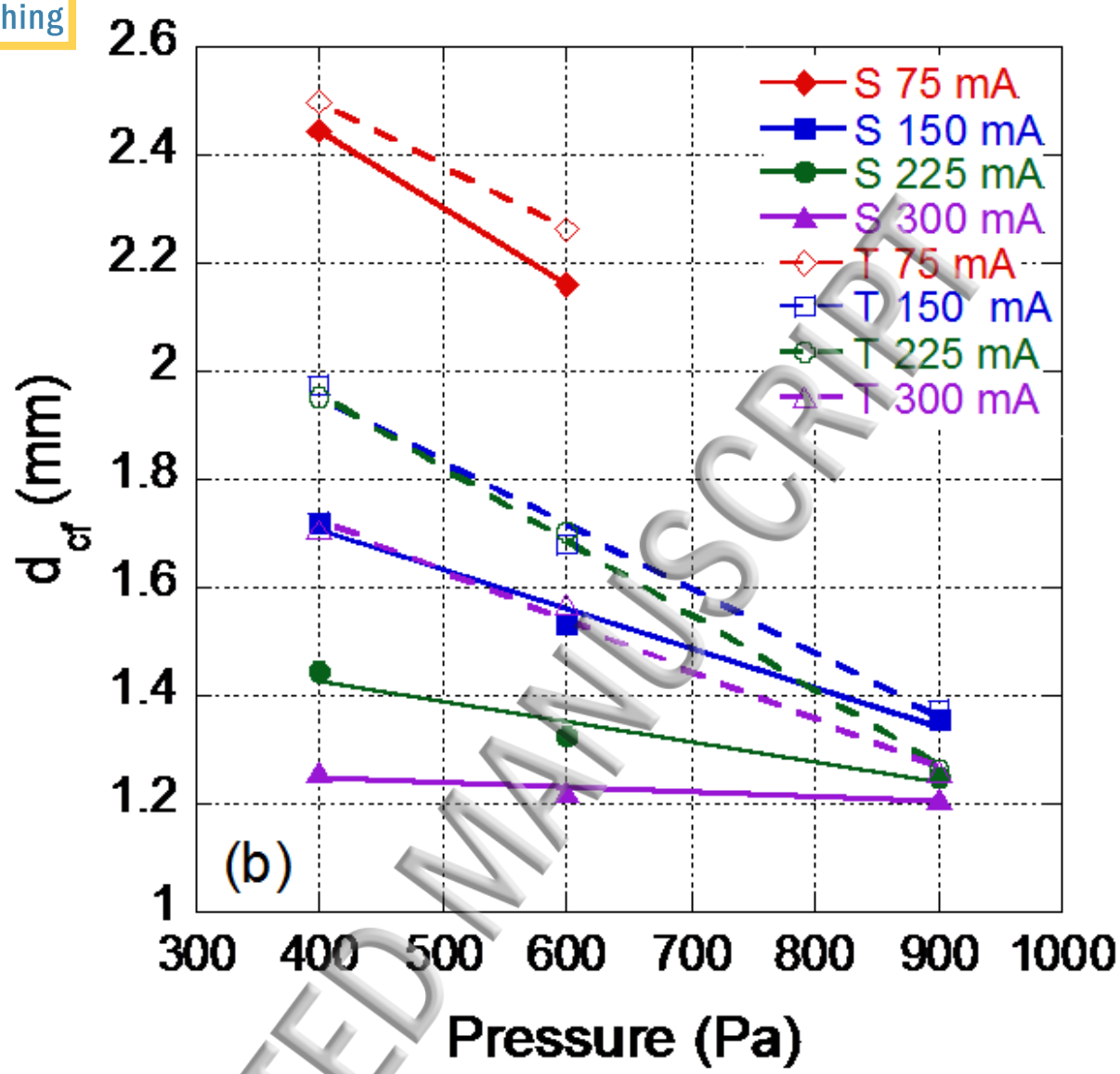

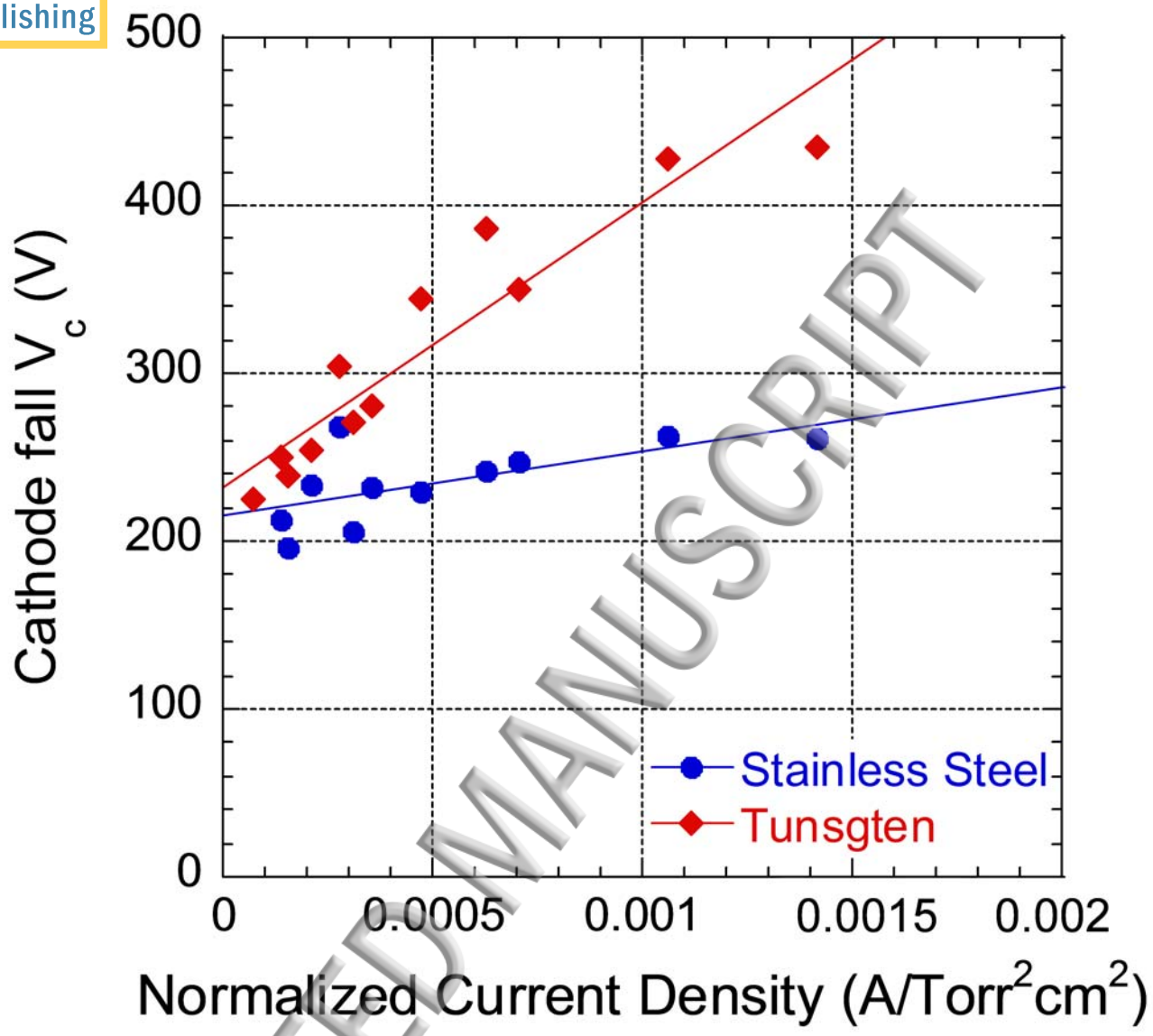

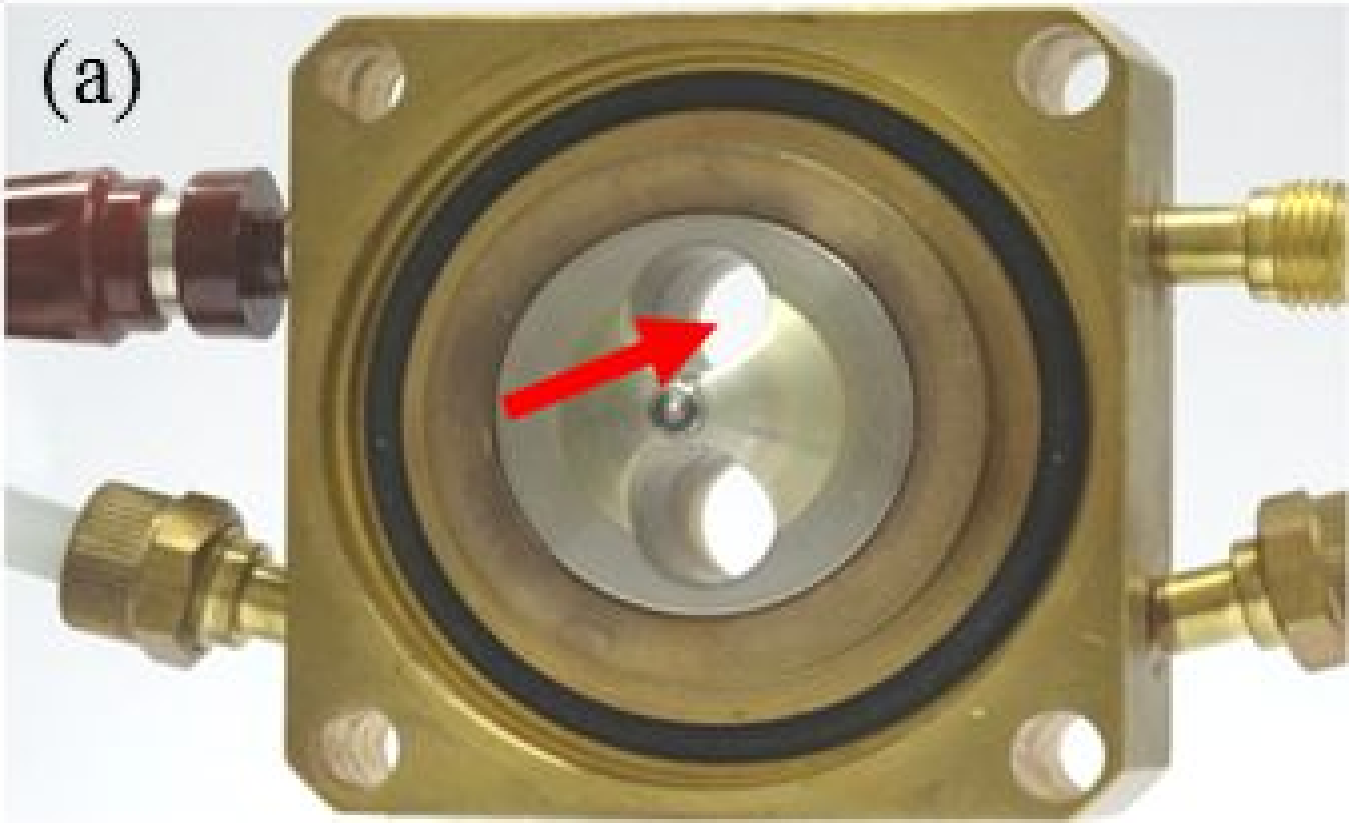
(a)

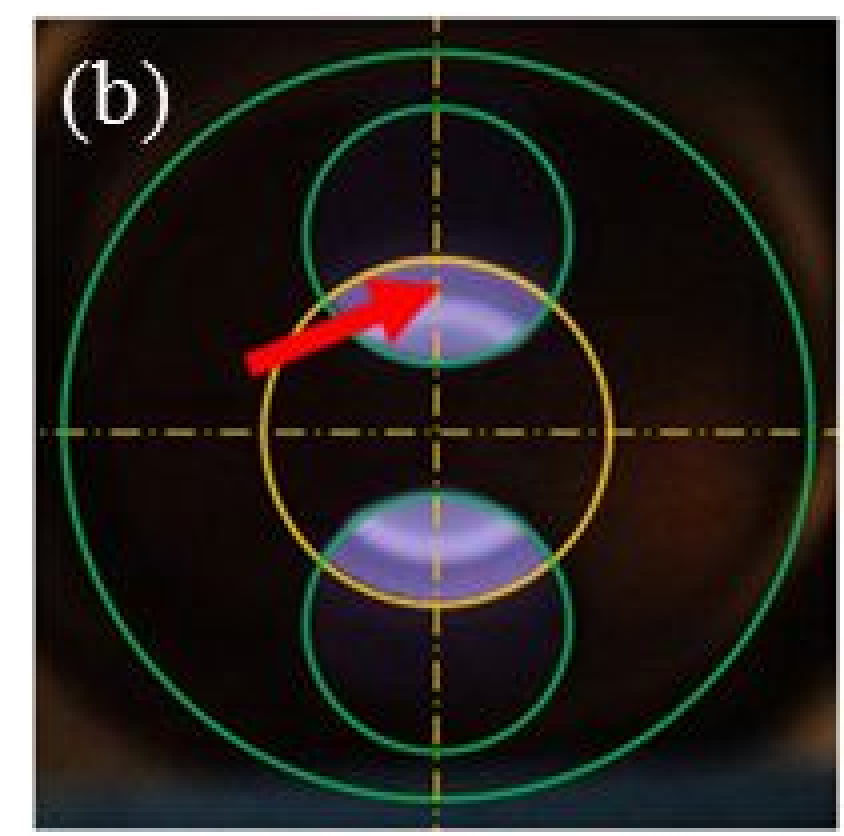
(b)